筋再生に伴うBMPシグナルの亢進

FOPでは，筋の損傷が異所性骨化を誘発する．野生型マウスの筋損傷・再生モデルを検討したところ，筋再生の過程でBMPの細胞内情報伝達因子であるSmad1とSmad5の発現が増加した[6]（図7），野生型ALK2はBMP非存在下ではSmad1/5を活性化しないが，FOPの変異ALK2受容体はBMP非存在下でもSmad1/5を活性化する（図7），したがって，FOPでは遺伝的に活性化されたALK2受容体と，筋再生によって局所的に増加したSmad1/5と相乗的に作用し，異所性骨形成が誘導される可能性がある[6]（図8）．

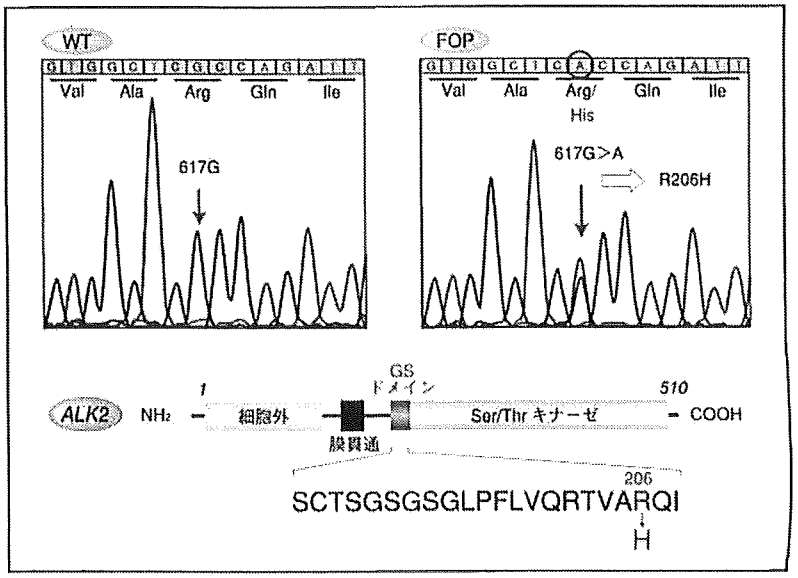

図5　FOPにおける*ACVR1*遺伝子の変異とALK2受容体の構造
野生型（WT）の*ACVR1*遺伝子は617番目の塩基がグアニンであるが，FOP患者では，ヘテロ接合体としてグアニンとアデニンのシグナルが検出される．この617番のG＞A変異は，ALK2受容体のGSドメインと呼ばれる領域の206番目のアルギニンをヒスチジンに変異させる．（筆者作成）

BMP受容体阻害剤によるFOP治療薬の開発

FOPの責任遺伝子がBMP受容体遺伝子であり，変異によって受容体が活性化されていることが予想された．これは，BMP受容体の阻害薬がFOPの治療薬として有効である可能性を示唆する．実際，培養細胞でDorsomorphinと命名された低分子のBMP受容体阻害薬が，FOPの変異ALK2活性を強力に抑制した[6]（図8），さらに，ALK2遺伝子に変異を導入した遺伝子改変マウスにおいても，Dorsomorphinの誘導体（LDN-193189）が異所性骨形成を抑制することが確認された[7]．

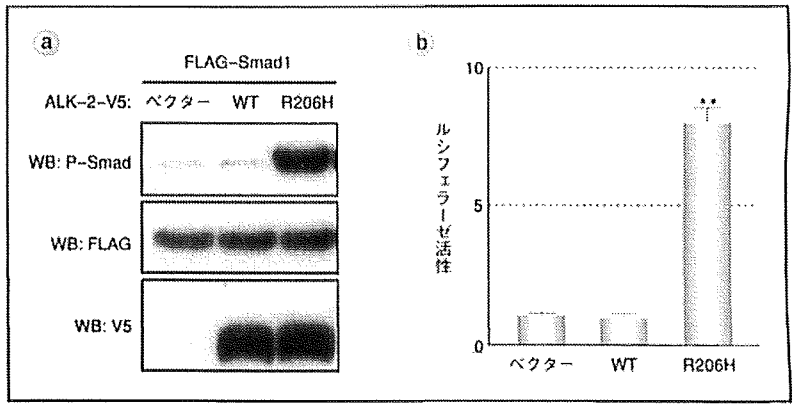

図6　FOPのALK2（R206H）は構成的活性型変異BMP受容体である
FOPで見出されたALK2（R206H）受容体は，BMP非存在下でもSmad1のリン酸化（a）と，*Smad*標的遺伝子の転写活性化（b）を誘導することから，構成的活性型であることが明らかとなった．
＊＊：$p < 0.01$．（文献6より改変）

FOPの遺伝子診断

FOPの発症を遅延させるためにも，早期に確定診断することが望まれるが，これまでFOPの診断法が確立されておらず，確定診断に平均4年以上を要していた[8]．しかし，FOPの責任遺伝子として*ACVR1*遺伝子が同定され，多くの症例が共通の遺伝子変異をもつことが明らかになり，FOPの遺伝子診断が可能となった．

典型的なFOP症例では，まだ筋組織に骨化が認められない出生時から，両足の親指に外反母趾様の変形が認められる．その後，2～5歳頃にはフレア・アップと呼ばれる腫瘤が頭部，頸部，背部，上腕などに認められる[9]．したがって，「外反母趾」と「フレア・

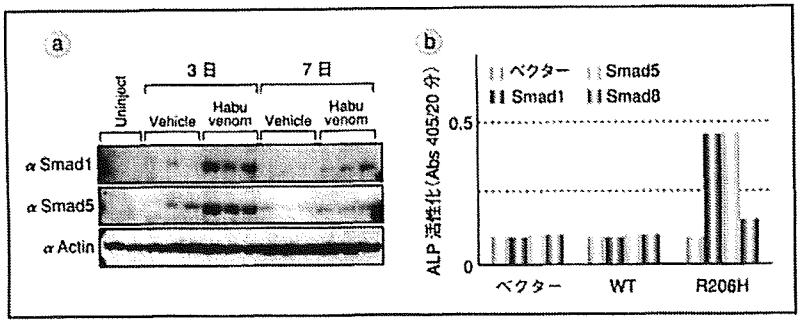

図7　筋再生に伴うSmad1/5の増加

マウスの大腿筋をハブ毒で破壊すると，数日以内にSmad1とSmad5の量が増加する(a)．さらに，FOPのALK2(R206H)受容体は，Smad1またはSmad5と相乗的に骨芽細胞分化を誘導する(b)．

(文献6より改変)

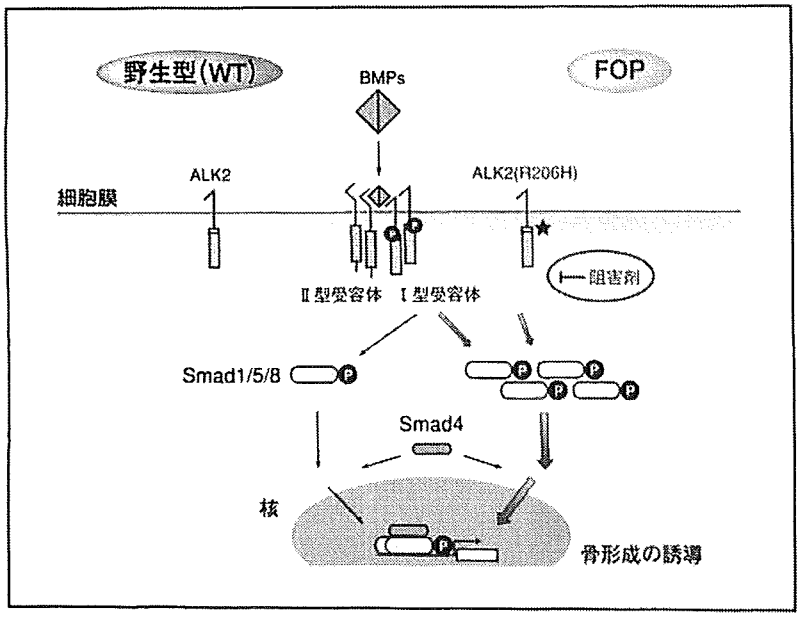

図8　FOPにおけるBMPシグナルの変異

野生型(WT)のALK2は，BMPと結合したときのみSmad1/5/8を介して骨形成を誘導する．一方，FOPのALK2(R206H)受容体は，GSドメインの変異によりBMP非存在下でも構成的にSmad1/5/8を活性化する．ALK2を阻害する分子は，FOPの治療に応用できる可能性がある．　(筆者作成)

アップ」が認められる症例は，まずFOPの可能性を疑い，生検などを実施する前に遺伝子診断を行うことが望まれる．

結語

最近の研究により，FOPが単一遺伝子の変異による疾患であることが明らかとなった．この発見に基づき，遺伝子診断の有効性や新しい治療標的が見出されている．今後，FOPの病態モデルが確立され，発症機序や治療薬の有効性などがさらに解明されることを期待したい．なお，紙面の都合上割愛したFOPに関する内容は，他の総説を参照されたい[9][10]．

謝辞

本稿は，埼玉医科大学ゲノム医学研究センター病態生理部門，埼玉医科大学FOP診療・研究プロジェクト，厚生労働省難治性疾患克服研究事業「脊柱靱帯骨化症に関する調査研究」班，「特定疾患患者の生活の質(Quality of Life；QOL)の向上に関する研究」班，「進行性骨化性線維異形成症(FOP)の生体資料の集積と新規治療法の開発に関する基盤研究」班から多大な協力を得たものであり，ここに感謝の意を表する．また，本研究の一部は，厚生労働科学研究費補助金，日本学術振興会科学研究費補助金，文部科学省私立大学戦略的研究基盤形成支援事業，埼玉医科大学学内グラント，武田生命科学振興財団，三共生命科学研究振興財団の助成を受けた．

References

1) Kaplan, F. S., Shen, Q., Lounev, V. et al.：*J. Bone Miner. Metab.* **26**：521-530, 2008
2) Katagiri, T., Suda, T., Miyazono, K.：The TGF-β Family (Miyazono, K., Derynck, R. eds.). Cold Spring Harbor Press, New York, 2008, pp.121-149
3) Katagiri, T., Yamaguchi, A., Komaki, M. et al.：*J. Cell Biol.* **127**：1755-1766, 1994
4) Shore, E. M., Xu, M., Feldman, G. J. et al.：*Nat. Genet.* **38**：525-527, 2006
5) Nakajima, M., Haga, N., Takikawa, K. et al.：*J. Hum. Genet.* **52**：473-475, 2007
6) Fukuda, T., Kohda, M., Kanomata, K. et al.：*J. Biol. Chem.* **284**：7149-7156, 2009
7) Yu, P. B., Deng, D. Y., Lai, C. S. et al.：*Nat. Med.* **14**：1363-1369, 2008
8) Kitterman, J. A., Kantanie, S., Rocke, D. M. et al.：*Pediatrics* **116**：e654-e661, 2005
9) 片桐岳信：内分泌・糖尿病科 **27**：270-276, 2008
10) 片桐岳信：日本医事新報 **4412**：70-74, 2008

日本未熟児新生児学会雑誌　第22巻　第1号　30～32頁（2010年）

●教育講演●

進行性骨化性線維異形成症(FOP)の発症メカニズムの解明と治療法

埼玉医科大学ゲノム医学研究センター　病態生理部門

片桐岳信

Key Words：muscle, heterotopic ossification, BMP receptor, ALK2

要　旨

進行性骨化性線維異形成症（FOP）は，筋組織内で異所性骨化が起こる遺伝性疾患である。筋組織の損傷が骨化を誘発することが知られており，侵襲的医療行為は禁忌とされるが，生検などによって骨化を招いた症例が多い。2006年にFOPの責任遺伝子として骨形成誘導因子の受容体であるALK2が同定された。FOP患者では，1塩基の変異によってアミノ酸変異が起こり，これによって受容体のリン酸化酵素がリガンド非依存的に活性化されて構成的に細胞内にシグナルが伝達されることが示された。これまでに，世界中のFOP患者から異なる10種類のALK2変異が同定された。これらの発見は，FOPがALK2単一遺伝子の変異に起因する疾患であり，異所性骨化の発症前でもALK2の遺伝子診断が有効なことを示唆している。

はじめに

進行性骨化性線維異形成症（Fibrodysplasia ossificans progressiva, FOP）は，成長に伴う全身の骨格筋や腱，靱帯などの異所性骨形成を特徴とする遺伝性疾患である[1)2)]。発症頻度は，世界的に約200万人に1人で，国内には約60人前後のFOP患者がいるものと推定されているが，未だ正確な数字は明らかでない。

FOPでは，進行により多くの関節が癒合するため，咀嚼を含む全身の可動域が極度に制限され，不自由な生活を余儀なくされる。現時点では，FOPの異所性骨化を抑制できる治療法は開発されておらず，骨化が始まると薬剤等で止めることができない。従って，FOPでは早期に確定診断し，可能な限り進行を遅延させることが重要である。

最近の研究により，FOPの責任遺伝子が明らかとなり，遺伝子診断が有効であることが示された。多くのFOP症例では，出生時から共通に認められるいくつかの症状が知られている。新生児と接する機会の多い医療従事者が，これらのFOPにおける特徴を共有することで，FOPの早期確定診断が可能となり，発症や進行を遅延させることが可能になるものと期待される。

別刷請求先：〒350-1241　埼玉県日高市山根1397-1
埼玉医科大学ゲノム医学研究センター
病態生理部門　片桐岳信

難病FOPの研究体制

FOPは，平成19年3月に開催された厚生労働省特定疾患対策懇談会において，難治性疾患克服研究事業対象疾患（いわゆる難病）の1つに認定された。これにより，別の異所性骨化を伴う疾患を対象としていた「脊柱靭帯骨化症に関する調査研究」班の中に，FOP研究グループが組織された。平成21年度は研究開始から3年目であり，6名の研究者を中心に国内のFOP患者数の調査，発症機序の解明，治療法の確立などに向けて研究が行われている。FOP研究班では，国内の医療従事者やFOP患者・家族に情報を提供する目的で，「FOP Newsletter」を定期的に刊行している。また，埼玉医科大学でも，FOPを専門に研究するための「FOP診療・研究プロジェクト」を組織し，FOPの克服に向けた研究に取り組んでいる。

世界的なFOP症例を対象としたアンケート調査によると，確定診断までに平均4年以上と平均6カ所の医療機関での受診を要している[3]。残念なことに，この間に生検や手術が行われた結果，急激な異所性骨形成を招いた症例が多い。これは，FOPの医学的情報が不足していたことに加え，FOPの診断法が確立されていなかったことによるところが大きい。

FOPの発症原因

1. 骨誘導因子BMPとFOP

FOPの異所性骨化と同様に，酸で脱灰した骨基質を筋組織や皮下に移植すると筋組織内で骨形成を誘発することが知られていた。これは，骨基質に含まれるBone Morphogenetic Protein（BMP）と呼ばれる成長因子の活性によるもので，BMPは筋芽細胞の培養系でも筋分化を阻害すると共に骨芽細胞様細胞への分化を誘導する[2)4)]。

BMPの骨誘導活性は，標的細胞の細胞膜上に発現した2種類の膜貫通型セリン・スレオニンキナーゼ受容体と，細胞質に存在するSmadと呼ばれる転写因子によって核へと伝達される[2)4)]。以前から，BMPの細胞内情報伝達系の異常がFOPを引き起こしている可能性が指摘されてきた。そして2006年，家族性FOPの連鎖解析から，FOPの責任遺伝子はACVR1遺伝子を含む第2染色体q23-24に局在することが同定された[5)]。

2. FOPの遺伝子変異

ACVR1遺伝子は，BMPのI型受容体であるALK2をコードする遺伝子で，世界的な家族性FOPと孤発性FOPの大部分は，ACVR1遺伝子の617番目の塩基がグアニンとアデニンのヘテロ接合体であることが判明した[5)~7)]。このACVR1遺伝子の617G＞A変異は，ALK2受容体の206番目のアルギニン残基をヒスチジンに置換（ALK2（R206H））させる。

さらに，臨床的な症状が従来の典型的FOPと異なるFOPから，新しいACVR1遺伝子の変異が同定されつつある。これまでに，10種類のALK2変異体が見出されている[8)~11)]。これまでに解析された我が国のFOP症例は，1例を除き全症例がALK2（R206H）であり，残る1例はALK2（G356D）であった[6)~8)]。

3. 変異ALK2による細胞内情報伝達系の活性化

FOPで見出された変異ALK2（R206H）を培養細胞に発現させると，BMP非存在下でも，Smadのリン酸化や標的遺伝子の転写が誘導される。また，変異受容体の過剰発現は筋分化を抑制し，骨芽細胞や軟骨細胞への分化を促進する[7)12)]。これらの結果は，ALK2(R206H)が，リガンド非依存的に活性化されたBMP受容体であることを示している。

4. FOPと筋再生

FOPでは，筋の損傷が異所性骨化を誘発する。これは，筋再生の過程でBMPの細胞内情報伝達因子の発現が増加することによる可能性がある。野生型マウスの筋損傷・再生モデルを検討すると，筋再生の過程でSmad1とSmad5の発現が増加した[7)]。ALK2(R206H)とSmad1またはSmad5を筋芽細胞で一緒に発現させると，BMPシグナルが伝達されたことから，FOPでは遺伝的に活性化されたALK2受容体と，筋再生によって局所的に増加したSmad1/5と相乗的に作用して，異所性骨形成が誘導される可能性がある[7)]。

FOPの遺伝子診断

FOPの骨化を抑制する治療法が確立されていない現状では，FOPを早期に診断し，進行を遅延させることが重要な課題である。前述のように，FOPの責任遺伝子としてACVR1/ALK2が同定されたことにより，遺伝子診断が可能となった。遺伝子診断は，迅速で，非侵襲的にサンプルを採取することが可能であり，骨化が起こる前でも確定診断が可能というFOPに有利な点がある。

典型的なFOP症例では，骨化が起こる前に認められる共通の特徴が明らかとなっている[1)3)]。1つは，まだ筋組織に骨化が認められない出生時から，両足の親指に左右対称性の外反母趾様変形が認められる点である。その後，2～5歳頃にはフレア・アップと呼ばれる腫瘤が頭部，頸部，背部，上腕などに認められる。多くの症例では，上部から下部へ，背部から前部へ，中心部から末梢へ，と骨化が進展することが知られている。

これらを考え合わせると，「出生時の外反母趾」と「フレア・アップ」が認められる症例はFOPの可能性を疑い，生検や手術などを実施する前にFOPの遺伝子

診断を行うことが望まれる。また，日常生活の中で事故により筋組織を損傷した結果，急性の異所性骨形成を発症した幼児の症例がある。フレア・アップの出現以前でもこうした事故は起こり得るため，外反母趾の場合には，早期にFOPを疑う必要性があるかも知れない。なお，FOP以外でどの程度外反母趾が出現するかは明らかでない。

FOP治療薬の開発

FOPの責任遺伝子がBMP受容体のACVR1/ALK2遺伝子で，変異ALK2が構成的に活性化されていることが明らかとなってきた。これらの発見を基に，BMP受容体を阻害するような化合物がFOP治療薬への応用を目指して研究されるようになっている。Dorsomorphinと命名された低分子のBMP受容体阻害薬は，FOPの変異ALK2活性を強力に抑制した[7]。さらに，ALK2遺伝子に変異を導入した遺伝子改変マウスにおいても，Dorsomorphinの誘導体（LDN-193189）が筋組織における異所性骨形成を抑制することが確認されている[13]。

おわりに

最近の研究により，FOPが単一遺伝子の変異による疾患であることが明らかとなった。この発見によって，FOPでは遺伝子診断が極めて有効であることが示された。今後は，この遺伝子診断の技術を生かすために，外反母趾のような特徴と遺伝子診断の有効性を，新生児や乳児と接する医療従事者に広めることが急務である。なお，紙面の都合上，割愛したFOPに関する内容は他の総説を参照されたい[14) 15)]。

本稿は，埼玉医科大学ゲノム医学研究センター病態生理部門，埼玉医科大学FOP診療・研究プロジェクト，厚生労働省難治性疾患克服研究事業「脊柱靱帯骨化症に関する調査研究」班，「特定疾患患者の生活の質（Quality of Life，QOL）の向上に関する研究」班，「進行性骨化性線維異形成症（FOP）の生体資料の集積と新規治療法の開発に関する基盤研究」班から多大な協力を得たものであり，ここに感謝の意を表する。また，本研究の一部は，厚生労働科学研究補助金，日本学術振興会科学研究補助金，文部科学省私立大学戦略的研究基盤形成支援事業，埼玉医科大学学内グラント，武田生命科学振興財団の助成を受けた。

文　献

1) Kaplan FS, Shen Q, Lounev V, et al. Skeletal metamorphosis in fibrodysplasia ossificans progressiva. J. Bone Miner. Metab 2008；26：521-530.
2) Katagiri T. Heterotopic ossification induced by bone morphogenetic protein signaling： fibrodysplasia ossificans progressiva. J. Oral Biosci, inpress.
3) Kitterman JA, Kantanie S, Rocke DM, et al. Iatrogenic harm caused by diagnostic errors in fibrodysplasia ossificans progressiva. Pediatrics 2005；116：e654-e661.
4) Katagiri T, Suda T, Miyazono K. The bone morphogenetic proteins. In The TGF-b Family. Miyazono K and Derynck R, editors. Cold Spring Harbor Press, New York, 2008；pp121-149.
5) Shore EM, Xu M, Feldman GJ, et al. A recurrent mutation in the BMP type I receptor ACVR1 causes inherited and sporadic fibrodysplasia ossificans progressiva. Nat. Genet 2006；38：525-527.
6) Nakajima M, Haga N, Takikawa K, et al. The ACVR1 617G > A mutation is also recurrent in three Japanese patients with fibrodysplasia ossificans progressiva. J. Hum. Genet 2007；52：473-475.
7) Fukuda T, Kohda M, Kanomata K, et al. Constitutively activated ALK-2 and increased Smad1/5 cooperatively induce BMP signaling in fibrodysplasia ossificans progressiva. J. Biol. Chem 2009；284：7149-7156.
8) Furuya H, Ikezoe K, Wang L, et al. A unique case of fibrodysplasia ossificans progressiva with an ACVR1 mutation, G356D, other than the common mutation (R206H). Am. J. Med. Genet. Part A 2008；146A：459-463.
9) Bocciardi R, Bordo D, Di Duca M, et al. Mutational analysis of the ACVR1 gene in Italian patients affected with fibrodysplasia ossificans progressiva：confirmations and advancements. Eur. J. Hum. Genet 2008；17：311-318.
10) Petrie KA, Lee WH, Bullock AN, et al. Novel mutations in ACVR1 result in atypical features in two fibrodysplasia ossificans progressiva patients. PLoS One 4：e5005.
11) Kaplan FS, Xu M, Seemann P, et al. Classic and atypical fibrodysplasia ossificans progressiva (FOP) phenotypes are caused by mutations in the bone morphogenetic protein (BMP) type I receptors ACVR1. Hum. Mut. 2009：30：379-390.
12) Shen Q, Little SC, Xu M, et al. The fibrodysplasia ossificans progressiva R206H ACVR1 mutation activates BMP-independent chondrogenesis and zebrafish embryo ventralization. J Clin Invest. 2009：119：3462-3472.
13) Yu PB, Deng DY, Lai CS, et al. BMP type I receptor inhibition prevents ectopic ossification in a mouse model of fibrodysplasia ossificans progressiva. Nat. Med 2008；14：1363-1369.
14) 片桐岳信．進行性骨化性線維異形成症（FOP）の病院と病態．内分泌・糖尿病科　2008；27：270-276.
15) 片桐岳信．進行性骨化性線維異形成症の病態と治療．日本医事新報　2008；4412：70-74.

Biochemical and Biophysical Research Communications 388 (2009) 648–653

Contents lists available at ScienceDirect

Biochemical and Biophysical Research Communications

journal homepage: www.elsevier.com/locate/ybbrc

Systematic gene regulation involving miRNAs during neuronal differentiation of mouse P19 embryonic carcinoma cell

Akiko Eda [1], Yoshiko Tamura [1], Mariko Yoshida, Hirohiko Hohjoh *

National Institute of Neuroscience, NCNP, 4-1-1 Ogawahigashi, Kodaira, Tokyo 187-8502, Japan

ARTICLE INFO

Article history:
Received 21 July 2009
Available online 11 August 2009

Keywords:
miRNA
let-7
Hmga2
Lin28
Neuronal differentiation

ABSTRACT

MicroRNAs (miRNAs) are small noncoding RNA and play an essential role in gene regulation. In this study, we investigated regulation of gene expression during neuronal differentiation of mouse P19 embryonic carcinoma cells and described a systematic pathway of gene regulation involving miRNAs. In the pathway, downregulation of *Lin28* involved in blocking the *let-7* maturation and upregulation of *let-7* occur following induction of the differentiation, thereby triggering suppression of the downstream *High Mobility Group A2* (*Hmga2*) gene expression via activation of gene silencing mediated by *let-7*. Our data further suggest that *miR-9*, as well as *miR-125b*, participate in the reduction of the *Lin28* expression. The gene regulation involving miRNAs likely contributes to a rapid and programmed change in gene expression in neuronal differentiation of P19 cells.

Introduction

MicroRNAs (miRNAs) are small noncoding RNA, with a length of 19–23 nt, which are processed from longer transcripts by digestion with Drosha in a complex with DGCR8/Pasha and Dicer in the nucleus and cytoplasm, respectively [1–3]. Hundreds of miRNA genes have been found in various species [3–5], and their tissue-specific expression has been detected [5–7]. Matured miRNAs are incorporated into the RNA-induced silencing complex (RISC) and function as mediators in gene silencing [8,9]. There are two types of suppression of gene expression involving miRNAs: one is the inhibition of translation of target mRNAs possessing partially complementary sequences to miRNAs in their 3′ untranslated regions (3′UTRs), and the other is the digestion of target RNAs which are perfectly or nearly complementary to miRNAs, such as RNA interference (RNAi). The gene silencing involving miRNAs appears to play an important role in regulation of gene expression in development, differentiation and proliferation [4,7,10–12]. Recent studies have further suggested significant association of miRNAs with various diseases[13,14].

The *let-7* miRNA was found in *Caenorhabditis elegans* for the first time as an RNA molecule that controls the developmental timing of progenitor cell maturation [15]. In mammal, several *let-7* members have been identified and belong together to the *let-7* family; and the expression of the *let-7* members appears to be developmentally controlled [16,17]. Recent studies have revealed that the *Lin28* gene encoding an RNA binding protein is involved in processing of *let-7* [18,19] and that the *High Mobility Group A2* (*Hmga2*) gene encoding a non-histone chromatin protein is a target for *let-7* [20,21]. In the current study, we investigated gene regulation involving miRNAs during neuronal differentiation of mouse P19 embryonic carcinoma cells, and described a systematic gene regulation involving the *let-7*, *miR-9* and *miR-125b* miRNAs. Our data suggest that the reduction of the Lin28 protein involving in part gene silencing mediated by *miR-9* and *miR-125b*, and the upregulation of *let-7* can trigger inhibition of the expression of the downstream *Hmga2* gene via gene silencing involving *let-7*.

Materials and methods

Cell culture. P19 and Neuro2a (N2a) cells were grown and neuronal differentiation of P19 cells were carried out as previously described [22].

Preparation of oligonucleotides. DNA and RNA oligonucleotides were obtained from BEX. For preparation of duplexes, sense- and antisense-strand oligonucleotides were mixed and annealed as described previously [23]. Sequences of synthesized DNA and RNA oligonucleotides are shown in related parts below. Non-silencing siRNA duplex (siControl; Qiagen) was used as the negative control.

DNA chip analysis. Total RNA was extracted from cultured cells using Trizol reagent (Invitrogen). For preparation of cellular miRNAs, small-sized RNAs containing miRNAs were isolated from total RNA using the RNeasy MinElute Cleanup kit (Qiagen). The isolated small-sized RNAs (~1 μg) were subjected to direct labeling with a fluorescent dye using the Platinum*Bright* 647 Infrared nucleic acid labeling kit (KREATECH), according to the manufac-

* Corresponding author. Fax: +81 42 346 1755.
E-mail address: hohjohh@ncnp.go.jp (H. Hohjoh).
[1] These authors contributed equally to this work.

0006-291X/$ - see front matter © 2009 Elsevier Inc. All rights reserved.
doi:10.1016/j.bbrc.2009.08.040

turer's instructions. After labeling, the labeled RNAs were purified from free fluorescent substrates by KREA*pure* columns (KREATECH) and used in hybridization. Hybridization was carried out with the *Genopal*®-MICM DNA chips (Mitsubishi Rayon) for detection of mouse miRNAs as described previously [22,24]. After hybridization, the DNA chips were washed twice in 2× SSC containing 0.2% SDS at 50 °C for 20 min followed by washing in 2 × SSC at 50 °C for 10 min, and then hybridization signals were examined by means of a DNA chip reader adopting multi-beam excitation technology according to the manufacturer's instructions (Yokogawa Electric Corporation).

Construction of reporter plasmids. To examine the effects of endogenous *miR-9* and *miR-125b* on gene silencing against *Lin28*, we constructed reporter plasmids with the psiCHECK-2 plasmid (Promega) encoding the *Renilla* and *Photinus luciferase* genes. The plasmid was digested with XhoI and NotI, and subjected to ligation with synthetic oligonucleotide duplexes carrying putative binding sites for *miR-9* and *miR-125b*, which exist in the *Lin28* 3′UTR. The resultant plasmids carry the target sequences in the 3′UTR of the *Renilla luciferase* gene. The sequences of the synthesized oligonucleotides are as follows:

mmLin28-miR9-Ss: 5′-TCGAGTCTCCATGTTTACTGCTAGAAACCAAAGCTA-3′
mmLin28-miR9-As: 5′-GGCCTAGCTTTGGTTTCTAGCAGTAAACATGGAGAC-3′
mmLin28-miR125b-Ss: 5′-TCGAGGTTCTCAGGTACATGAGCAATCTCAGGGATA-3′
mmLin28-miR125b-As: 5′-GGCCTATCCCTGAGATTGCTCATGTACCTGAGAACC-3′

We also used the reporter plasmids constructed in the previous study [25]. The plasmids (using psiCHECK-2 as a backbone plasmid) carry perfectly matched target sequence (PMTS) and three bulged binding sites (3xBBS) for *let-7* in the 3'UTR of the *Renilla luciferase* gene.

Transfection and reporter assay. Transfection of the reporter plasmids using Lipofectamine 2000 transfection reagent (Invitrogen) and luciferase assay with the Dual-Luciferase reporter assay system (Promega) were carried out according to the manufacturer's instructions. The reporter plasmids were also transfected together with Pre-miR miRNA precursor of *miR-9* (PM10022; Ambion), *miR-125b* (PM10148; Ambion) or negative control#1 (Ambion) into cells.

Introduction of the Pre-miR miRNA precursor of *let-7a* (PM10048; Ambion), siRNA targeting *Lin28* (siLin28) and non-silencing siRNA duplex (siControl; Qiagen) into P19 cells was carried out by means of a Nucleofector system (Amaxa Biosystems) according to the manufacturer's instructions. The sequences of the synthesized siRNAs were as follows:

siLin28-ss: 5′-GGGUUGUGAUGACAGGCAAUU-3′
siLin28-as: 5′-UUGCCUGUCAUCACAACCCUU-3′

Western blot. Equal amounts of proteins were separated by SDS–PAGE and electrophoretically blotted onto PVDF membranes (Millipore). Membranes were blocked in blocking solution (5% non-fat milk and 0.05% Tween-20 in PBS) and incubated with rabbit polyclonal anti-HMGA2-P3 antibody (59210AP; BIOCHECK), anti-Lin28 antibody (ab63740; Abcom), or goat polyclonal anti-Actin antibody (sc-1616; Santa Cruz Biotechnology), followed by washing in PBS containing 0.05% Tween-20, and then further incubated with horseradish peroxidase-conjugated anti-rabbit or anti-goat IgG. Antigen–antibody complexes were visualized using chemiluminescent reagent (Millipore).

Fractionation of nuclear and cytoplasmic RNAs. Cells were washed with phosphate-buffered saline solution (PBS) twice, harvested, resuspended in cell lysis buffer containing 20 mM HEPES (pH 7.5), 150 mM NaCl, 10 mM $MgCl_2$, 1 mM EDTA and 0.5% NP-40, and placed on ice for 10 min. The cell extract was subjected to centrifugation at 800*g* for 10 min. Total RNAs were extracted from the sedimented pellet (containing nuclei) and supernatant (a crude cytoplasmic fraction) using Trizol reagent (Invitrogen).

Reverse transcription – (real time) polymerase chain reaction (Q-PCR). Total RNA was treated with Turbo DNase I (Ambion) and subjected to RT- (real time) PCR (Q-PCR). Q-PCR was performed by means of the AB 7300 Real Time PCR System (Applied Biosystems) with a TaqMan Universal PCR Master Mix together with TaqMan® Gene Expression Assays or TaqMan® MicroRNA Assays (Applied Biosystems) or a SYBR Green PCR Master Mix together with Perfect Real Time Primers (TAKARA BIO), according to the manufacturer's instructions.

End-point PCR analysis for *let-7a*, *let-7g* and *5sRNA* as a control was carried out by means of the GeneAmp PCR system 9700 (Applied Biosystems) with the mirVana qRT-PCR detection kit (Ambion) and primer sets (Ambion) according to the manufacturer's instructions. The resultant PCR products were electrophoretically separated on 12% polyacrylamide gels and visualized by ethidium bromide staining.

TaqMan® Gene Expression Assays used in this study were as follows (Assay ID): Gapdh (Mm99999915_g1).

TaqMan® MicroRNA Assays used were as follows (Assay ID): hsa-let-7a (377), hsa-let-7b (378), hsa-let-7c (379), hsa-let-7 g (383) and snoRNA202 (1232).

Perfect Real Time Primers used were as follows (Primer-Set ID): *Hmga2* (MA066259-F/R), *Lin28* (MA077408-F/R), and *Gapdh* (MA05 0371-F/R).

We also synthesized the PCR primers for the *let-7g* primary transcript and *Hmga2* according to the previous studies [17,26], and used the PCR primers for *Pou5f1* in our previous study[22].

Results and discussion

Control of Hmga2 expression by gene silencing during neuronal differentiation of P19 cells

P19 mouse embryonal carcinoma cells can be induced to differentiate into neuronal cells by retinoic acid (RA), and the cells treated with RA show a dramatic change in expression of genes including miRNAs [22,27]. In the current study, we examined the expression of *let-7* miRNA and its target gene, *High Mobility Group A2* (*Hmga2*) carrying seven putative binding sites for *let-7* in its 3'UTR during neuronal differentiation of P19 cells using RT-PCR and Western blotting (Fig. 1A). The results indicated that: (i) *let-7a* markedly increased in its expression level during the neuronal differentiation, (ii) the *Hmga2* transcript and protein existed in undifferentiated P19 cells (lane UD), (iii) the protein was detectable at the beginning of RA treatment, but (iii) it was markedly reduced on day 4 (96 h) and hardly detected in the completely differentiated P19 neurons, and interestingly, (iv) the level of the *Hmga2* transcript appeared to remain unchanged throughout the differentiation. DNA chip analysis further demonstrated that not only *let-7a* but also other *let-7* members (*let-7b-g* and *-7i*) were markedly increased during the differentiation (Supplementary Fig. s1); and consistently, a reporter gene assay revealed that gene silencing activity mediated by endogenous *let-7* was enhanced after RA treatment (Supplementary Fig. s2). To further confirm the results, synthetic (exogenous) pre-*let-7a* precursor was introduced into undifferentiated P19 cells expressing little *let-7*, and the expression of the *Hmga2* transcript and protein was examined. As expected, the results revealed that the Hmga2 protein was reduced in the presence of the pre-*let-7* precursor, although the *Hmga2* transcript remained unchanged (Fig. 1B–E). The data presented here are

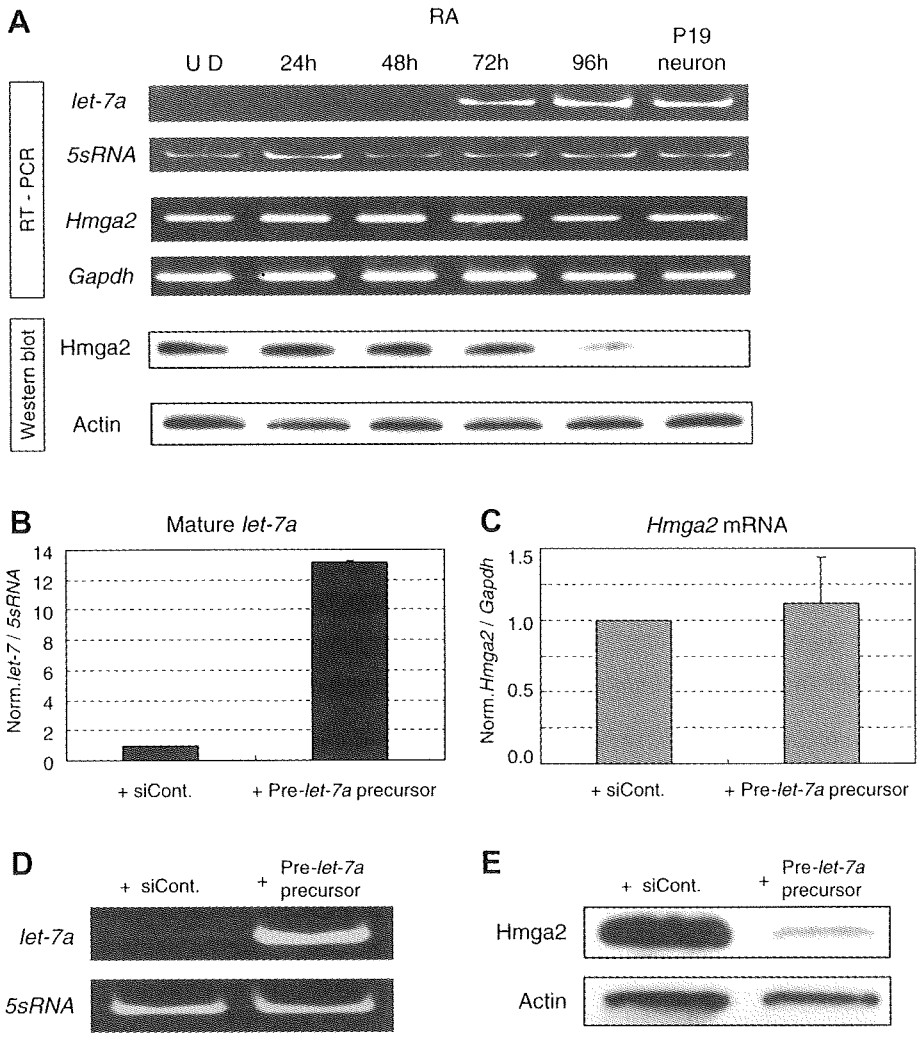

Fig. 1. Expression profiles of *let-7* and target *Hmga2* gene during neuronal differentiation of P19 cells and inhibition of the Hmga2 expression by synthetic *pre-let-7a* precursor. (A) Total RNA and protein were prepared from undifferentiated P19 cells (UD) at the indicated time points after induction of differentiation with retinoic acid (RA) and completely differentiated P19 neurons, and then examined by RT-PCR and Western blot analyses. Examined RNAs and proteins are indicated. *5sRNA* and *Gapdh* in RT-PCR and Actin in Western blot were studied as controls. (B-E) Synthetic Pre-miR miRNA precursor of *let-7a* (Pre-*let-7a* precursor) and siControl (siCont.) were introduced into undifferentiated P19 cells by means of a Nucleofector system (Amaxa Biosystems). Two days after transfection, total RNA and cell lysate were prepared. RNA levels of mature *let-7a* (B) and *Hmga2* (C) were examined by Q-PCR and normalized by those of *5sRNA* and *Gapdh*, respectively, and then the ratios of the RNA levels were normalized against the ratios obtained in the presence of siControl (siCont.). Data are the means of three repeated determinations. Error bars represent standard deviations. (D) End-point PCR analysis of *B* was carried out as described in Materials and Methods. (E) Western blot analysis of Hmga2 was carried out as in *A*.

compatible with the previous results [20,21]. Taken together, the evidence suggests that expression of the Hmga2 protein during neuronal differentiation of P19 cells is probably regulated by gene silencing mediated by endogenous *let-7*, which is further controlled by the differentiation.

Relationship between Lin28 and let-7 during neuronal differentiation

Recent studies have shown that Lin28, a developmentally regulated RNA binding protein, can block the processing of *pre-let-7* miRNAs [18,19]. Then we examined the expression of the *Lin28* transcript and protein together with the *let-7g* primary transcript and mature *let-7g* during neuronal differentiation of P19 cells. As shown in Fig. 2, mature *let-7g* was increased with decreased expression of either the *Lin28* transcript or its protein, whereas the *let-7g* primary transcript appeared to remain unchanged over the course of differentiation; the data are consistent with the previous studies [19,28]. To further investigate if there are any associations between Lin28 and the *let-7* family members and between Lin28 and miRNAs other than *let-7*, expression profiles of miRNAs in *Lin28* knockdown (Supplementary Fig. s3) and naïve P19 cells were examined by means of DNA chips and RT-real time PCR (Q-PCR). The results indicated that all the *let-7* family members were significantly increased in the *Lin28* knockdown P19 cells as compared with those in negative control cells (Q-PCR data in Supplementary Fig. s3D). As for other associations, neither significant increase nor decrease in miRNAs other than the *let-7* family members was detected in the *Lin28* knockdown P19 cells from our current study (data not shown).

We next examined the *Hmga2* transcript and protein in the *Lin28* knockdown P19 cells by RT-semi-quantitative PCR and Western blotting, respectively. As a result, no significant difference in either the RNA or protein was detected between the knockdown and naïve P19 cells (Supplementary Fig. s3A and C). Since the level of mature *let-7* in the knockdown cells was still rather lower than that in RA-treated or pre-*let-7a* transfected P19 cells (Fig. 1B), insufficient level of mature *let-7* may account for the results. Accordingly, it is conceivable that the reduction of Lin28 and also the upregulation of *let-7* are required for exerting gene silencing mediated by *let-7* in differentiating P19 cells.

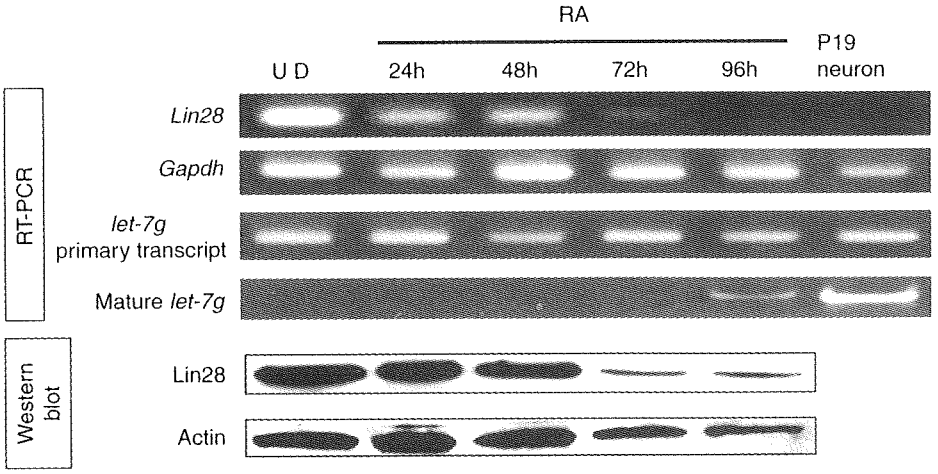

Fig. 2. Expression profiles of *Lin28* and *let-7g* during neuronal differentiation of P19 cells. RT-PCR and Western blot analyses were carried out as in Fig. 1. Examined gene products are indicated.

Contribution of miR-9 and miR-125b to the reduction of the Lin28 mRNA

Based on the present and previous studies, the reduction of Lin28 appears to be necessary for triggering inhibition of translation of *Hmga2* at a programmed time in differentiating P19 cells. Then, how is the *Lin28* gene expression regulated during the differentiation? We investigated the *Lin28* transcript in the nuclei and cytoplasm of RA-treated P19 cells by RT semi-quantitative PCR. As shown in Fig. 3, intriguing results were obtained: the level of the *Lin28* transcript in the cytoplasmic fraction decreased 48 h after RA treatment, whereas the transcript in the nuclear fraction was markedly reduced 72 h after RA treatment (Fig. 3); *i.e.*, the initial degradation of the RNA occurred in the cytoplasmic fraction, but not in the nuclear fraction. In contrast, the *Pou5f1* (*Oct3/4*) RNA studied as a control showed its initial reduction in the nuclear fraction (24 h) followed by the reduction in the cytoplasmic fraction (48 h), suggesting the loss of promoter activity as a possible primary cause. From the results, it is conceivable that not only promoter activity (in the nucleus) but also post-transcriptional regulation (in the cytoplasm) is involved in the reduction of the *Lin28* transcript in RA-treated (differentiating) P19 cells.

We focused on the reduction of the *Lin28* transcript in the cytoplasm. The previous report suggested that *miR-125b* could regulate the *Lin28* gene expression through gene silencing [28]. Our current study with miRNA expression profiles and the *in silico* analysis

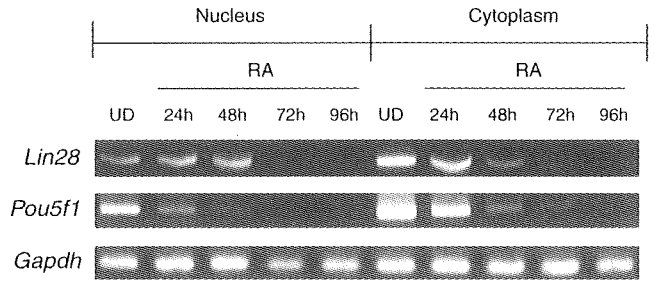

Fig. 3. Expression levels of *Lin28*, *Pou5f1* and *Gapdh* in nucleus and cytoplasm. Cell lysate was prepared from P19 cells at the indicated time points after induction of differentiation with RA and fractionated by centrifugation at 800*g* into the sediments (containing abundant nuclei) and supernatants (a crude cytoplasmic fraction). RNAs extracted from the sediments (nucleus) and supernatants (cytoplasm) were subjected to reverse transcription for synthesizing the first strand cDNA with random primers and oligo(dT) primer, respectively, and examined by semi-quantitative PCR using primers specific for indicated genes.

using the TargetScan program further predicted a candidate, *miR-9*, other than *miR-125b*, having the potential for regulating the *Lin28* gene expression: putative binding sites for *miR-9* and *miR-125b* are present in the *Lin28* 3′UTR and their expression is upregulated after RA treatment (Supplementary Fig. s1). To assess the association between the miRNAs and *Lin28*, we constructed reporter plasmids carrying the putative binding sites for *miR-9* and *miR-125b* in the 3′UTR of the *Renilla luciferase* gene. When the reporter plasmids together with synthetic pre-*miR-9* or pre-*miR-125b* precursor were introduced into naïve P19 and Neuro2a (N2a) cells, which hardly express both miR-9 and miR-125b, a sequence-specific gene silencing of the introduced miRNAs to the target reporter genes was detected (Fig. 4A and B), suggesting that the examined sequences (introduced into the reporter gene) carry the authentic binding sites for the miRNAs. Then we introduced the reporter plasmids into RA-treated P19 cells. The results indicated that the expression of the reporter gene carrying the target sequences was significantly decreased in the cells (Fig. 4C), where *miR-9* and *miR-125b* appear to be upregulated (Supplementary Fig. s1). It should be noted that the reporter gene carrying the *miR-9* target sequence (miR-9TS) looked like undergoing suppression stronger than the reporter gene with the *miR-125b* target sequence (miR-125bTS) (Fig. 4C). Since *miR-9* appears to be upregulated earlier and more abundant than *miR-125b* in RA-treated P19 cells (Supplementary Fig. s1), these may account for the difference in suppression level between them. Consequently, *Lin28* is likely subjected to gene silencing involving *miR-9* and *miR-125b* during neuronal differentiation of P19 cells.

Systematic gene regulation involving gene silencing during neuronal differentiation

The present and previous studies suggest that a systematic gene regulation involving gene silencing takes place during neuronal differentiation of P19 cells (Supplementary Fig. s4): (i) various genes including *miR-9* and *miR-125b* are upregulated after RA treatment for induction of the differentiation; (ii) *Lin28* blocking the *let-7* maturation is subjected to gene silencing mediated by *miR-9* and *miR-125*; and its promoter activity is also downregulated; (iii) the reduction of the Lin28 protein permits processing of *let-7* and the *let-7* genes themselves are also upregulated, thereby accumulating mature *let-7* in the cells; (iv) the matured *let-7* is incorporated into RISC; and (v) the resultant RISC initiates inhibition of the expression of the Hmga2 protein without reduction of the *Hmga2* transcript. Give that Hmga2 appears to participate in

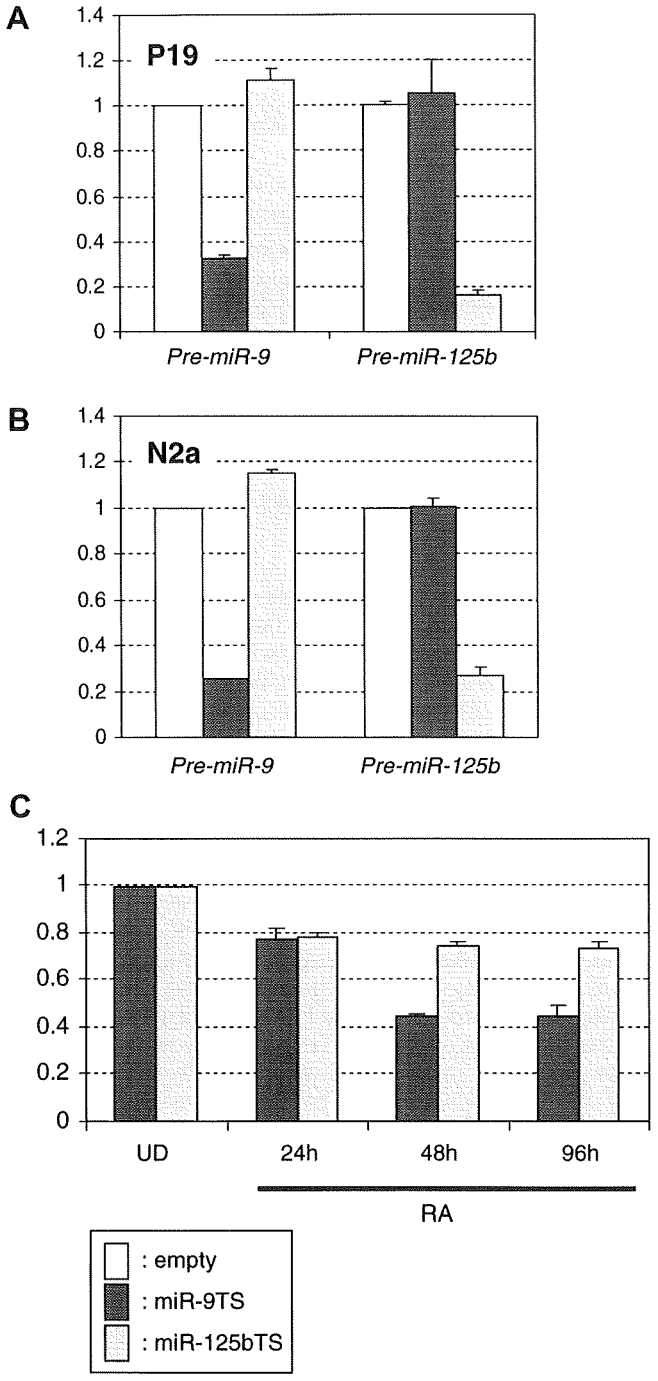

Fig. 4. Reporter gene assay. (A,B) Reporter plasmids carrying the predicted *miR-9* (miR-9TS) and *miR-125b* (miR-125bTS) target sequences in the 3'UTR of the *Renilla luciferase* gene and an empty plasmid (empty) as a control were introduced together with synthetic pre-miR-9 or pre-miR-125b precursor into undifferentiated P19 (A) and Neuro2a (N2a) (B) cells. Twenty-four hours after transfection, cell lysate was prepared and dual luciferase assay was carried out. Ratios of normalized target (Renilla) luciferase activity to control (Photinus) luciferase activity are shown: the ratios of luciferase activity determined with the plasmids carrying the miR-9TS and miR-125bTS are normalized to the ratio obtained with the control (empty) plasmid. Data are averages of three independent experiments. Error bars represent standard deviations. (C) The reporter plasmids were also transfected into RA-treated P19 cells. P19 cells were treated with RA for indicated hours and subjected to transfection thereafter. Dual luciferase assay was carried out as in A. Ratios of normalized target luciferase activity to control activity are indicated: the ratios of luciferase activity determined in RA-treated P19 cells are normalized to the ratio obtained in naive (undifferentiated) cells. Data are averages of three independent experiments. Error bars indicate standard deviations.

self-renewal and stemness [29,30], the gene regulation described above may contribute to a swift silencing of *Hmga2* and a rapid differentiation of P19 cells.

Acknowledgments

This work was supported in part by research grants from the Ministry of Health, Labour and Welfare of Japan and by Grants-in-Aid for Scientific Research from the Japan Society for the Promotion of Science.

Appendix A. Supplementary data

Supplementary data associated with this article can be found, in the online version, at doi:10.1016/j.bbrc.2009.08.040.

References

[1] Y. Lee, C. Ahn, J. Han, H. Choi, J. Kim, J. Yim, J. Lee, P. Provost, O. Radmark, S. Kim, V.N. Kim, The nuclear RNase III Drosha initiates microRNA processing, Nature 425 (2003) 415–419.
[2] A.M. Denli, B.B. Tops, R.H. Plasterk, R.F. Ketting, G.J. Hannon, Processing of primary microRNAs by the microprocessor complex, Nature 432 (2004) 231–235.
[3] D.P. Bartel, MicroRNAs: genomics, biogenesis, mechanism, and function, Cell 116 (2004) 281–297.
[4] A.M. Krichevsky, K.S. King, C.P. Donahue, K. Khrapko, K.S. Kosik, A microRNA array reveals extensive regulation of microRNAs during brain development, RNA 9 (2003) 1274–1281.
[5] M. Lagos-Quintana, R. Rauhut, A. Yalcin, J. Meyer, W. Lendeckel, T. Tuschl, Identification of tissue-specific microRNAs from mouse, Curr. Biol. 12 (2002) 735–739.
[6] T. Babak, W. Zhang, Q. Morris, B.J. Blencowe, T.R. Hughes, Probing microRNAs with microarrays: tissue specificity and functional inference, RNA 10 (2004) 1813–1819.
[7] C.G. Liu, G.A. Calin, B. Meloon, N. Gamliel, C. Sevignani, M. Ferracin, C.D. Dumitru, M. Shimizu, S. Zupo, M. Dono, H. Alder, F. Bullrich, M. Negrini, C.M. Croce, An oligonucleotide microchip for genome-wide microRNA profiling in human and mouse tissues, Proc. Natl. Acad. Sci. USA 101 (2004) 9740–9744.
[8] G. Hutvagner, P.D. Zamore, A microRNA in a multiple-turnover RNAi enzyme complex, Science 297 (2002) 2056–2060.
[9] R.S. Pillai, S.N. Bhattacharyya, C.G. Artus, T. Zoller, N. Cougot, E. Basyuk, E. Bertrand, W. Filipowicz, Inhibition of translational initiation by Let-7 MicroRNA in human cells, Science 309 (2005) 1573–1576.
[10] J.G. Doench, C.P. Petersen, P.A. Sharp, SiRNAs can function as miRNAs, Genes Dev. 17 (2003) 438–442.
[11] Y. Zeng, R. Yi, B.R. Cullen, MicroRNAs and small interfering RNAs can inhibit mRNA expression by similar mechanisms, Proc. Natl. Acad. Sci. USA 100 (2003) 9779–9784.
[12] A.M. Cheng, M.W. Byrom, J. Shelton, L.P. Ford, Antisense inhibition of human miRNAs and indications for an involvement of miRNA in cell growth and apoptosis, Nucleic Acids Res. 33 (2005) 1290–1297.
[13] S.A. Waldman, A. Terzic, A study of microRNAs in silico and in vivo: diagnostic and therapeutic applications in cancer, FEBS J. 276 (2009) 2157–2164.
[14] M.S. Weinberg, M.J. Wood, Short non-coding RNA biology and neurodegenerative disorders: novel disease targets and therapeutics, Hum. Mol. Genet. 18 (2009) R27–R39.
[15] V. Ambros, The functions of animal microRNAs, Nature 431 (2004) 350–355.
[16] F.G. Wulczyn, L. Smirnova, A. Rybak, C. Brandt, E. Kwidzinski, O. Ninnemann, M. Strehle, A. Seiler, S. Schumacher, R. Nitsch, Post-transcriptional regulation of the let-7 microRNA during neural cell specification, FASEB J. 21 (2007) 415–426.
[17] J.M. Thomson, M. Newman, J.S. Parker, E.M. Morin-Kensicki, T. Wright, S.M. Hammond, Extensive post-transcriptional regulation of microRNAs and its implications for cancer, Genes Dev. 20 (2006) 2202–2207.
[18] I. Heo, C. Joo, J. Cho, M. Ha, J. Han, V.N. Kim, Lin28 mediates the terminal uridylation of let-7 precursor MicroRNA, Mol. Cell 32 (2008) 276–284.
[19] S.R. Viswanathan, G.Q. Daley, R.I. Gregory, Selective blockade of microRNA processing by Lin28, Science 320 (2008) 97–100.
[20] C. Mayr, M.T. Hemann, D.P. Bartel, Disrupting the pairing between let-7 and Hmga2 enhances oncogenic transformation, Science 315 (2007) 1576–1579.
[21] Y.S. Lee, A. Dutta, The tumor suppressor microRNA let-7 represses the HMGA2 oncogene, Genes Dev. 21 (2007) 1025–1030.
[22] H. Hohjoh, T. Fukushima, Marked change in microRNA expression during neuronal differentiation of human teratocarcinoma NTera2D1 and mouse embryonal carcinoma P19 cells, Biochem. Biophys. Res. Commun. 362 (2007) 360–367.
[23] Y. Ohnishi, K. Tokunaga, H. Hohjoh, Influence of assembly of siRNA elements into RNA-induced silencing complex by fork-siRNA duplex carrying nucleotide

mismatches at the 3′- or 5′-end of the sense-stranded siRNA element, Biochem. Biophys. Res. Commun. 329 (2005) 516–521.
[24] H. Hohjoh, T. Fukushima, Expression profile analysis of microRNA (miRNA) in mouse central nervous system using a new miRNA detection system that examines hybridization signals at every step of washing, Gene 391 (2007) 39–44.
[25] Y. Tamura, M. Yoshida, Y. Ohnishi, H. Hohjoh, Variation of gene silencing involving endogenous microRNA in mammalian cells, Mol. Biol. Rep. 36 (2009) 1413–1420.
[26] T. Sanosaka, M. Namihira, H. Asano, J. Kohyama, K. Aisaki, K. Igarashi, J. Kanno, K. Nakashima, Identification of genes that restrict astrocyte differentiation of midgestational neural precursor cells, Neuroscience 155 (2008) 780–788.
[27] L.F. Sempere, S. Freemantle, I. Pitha-Rowe, E. Moss, E. Dmitrovsky, V. Ambros, Expression profiling of mammalian microRNAs uncovers a subset of brain-expressed microRNAs with possible roles in murine and human neuronal differentiation, Genome Biol. 5 (2004) R13.
[28] L. Wu, J.G. Belasco, Micro-RNA regulation of the mammalian lin-28 gene during neuronal differentiation of embryonal carcinoma cells, Mol. Cell. Biol. 25 (2005) 9198–9208.
[29] J. Nishino, I. Kim, K. Chada, S.J. Morrison, Hmga2 promotes neural stem cell self-renewal in young but not old mice by reducing p16Ink4a and p19Arf Expression, Cell 135 (2008) 227–239.
[30] F. Yu, H. Yao, P. Zhu, X. Zhang, Q. Pan, C. Gong, Y. Huang, X. Hu, F. Su, J. Lieberman, E. Song, Let-7 regulates self renewal and tumorigenicity of breast cancer cells, Cell 131 (2007) 1109–1123.

Human Molecular Genetics, 2009, Vol. 18, No. 19 **3708–3724**
doi:10.1093/hmg/ddp318
Advance Access published on July 15, 2009

Three human *ARX* mutations cause the lissencephaly-like and mental retardation with epilepsy-like pleiotropic phenotypes in mice

Kunio Kitamura[1,3,*], Yukiko Itou[1,†], Masako Yanazawa[3,†], Maki Ohsawa[1,†,‡], Rika Suzuki-Migishima[3], Yuko Umeki[1], Hirohiko Hohjoh[2], Yuchio Yanagawa[4], Toshikazu Shinba[5], Masayuki Itoh[1], Kenji Nakamura[3] and Yu-ichi Goto[1]

[1]Department of Mental Retardation and Birth Defect Research and [2]Department of Molecular Genetics, National Institute of Neuroscience, National Center of Neurology and Psychiatry, Tokyo, Japan, [3]Mitsubishi Kagaku Institute of Life Sciences, Tokyo, Japan, [4]Department of Genetic and Behavioral Neuroscience, Gunma University Graduate School of Medicine, Gunma, Japan and [5]Stress Disorders Research Team, Tokyo Institute of Psychiatry, Tokyo, Japan

Received March 29, 2009; Revised June 8, 2009; Accepted July 9, 2009

***ARX* (the *aristaless*-related homeobox gene) is a transcription factor that participates in the development of GABAergic and cholinergic neurons in the forebrain. Many *ARX* mutations have been identified in X-linked lissencephaly and mental retardation with epilepsy, and thus *ARX* is considered to be a causal gene for the two syndromes although the neurobiological functions of each mutation remain unclear. We attempted to elucidate the causal relationships between individual *ARX* mutations and disease phenotypes by generating a series of mutant mice. We generated three types of mice with knocked-in *ARX* mutations associated with X-linked lissencephaly (P353R) and mental retardation [P353L and 333ins(GCG)7]. Mice with the P355R mutation (equivalent to the human 353 position) that died after birth were significantly different in *Arx* transcript/protein amounts, GABAergic and cholinergic neuronal development, brain morphology and lifespan from mice with P355L and 330ins(GCG)7 but considerably similar to *Arx*-deficient mice with truncated *ARX* mutation in lissencephaly. Mice with the 330ins(GCG)7 mutation showed severe seizures and impaired learning performance, whereas mice with the P355L mutation exhibited mild seizures and only slightly impaired learning performance. Both types of mutant mice exhibited the mutation-specific lesser presence of GABAergic and cholinergic neurons in the striatum, medial septum and ventral forebrain nuclei when compared with wild-type mice. Present findings that reveal a causal relationship between *ARX* mutations and the pleiotropic phenotype in mice, suggest that the *ARX*-related syndrome, including lissencephaly or mental retardation, is caused by only the concerned *ARX* mutations without the involvement of other genetic factors.**

INTRODUCTION

The forebrain comprises a number of functionally and morphologically distinct types of neurons that, in coordination, regulate various aspects of cognition and behavior. *ARX*, thought to play an important role in forebrain development, is conserved in vertebrates and the ARX protein contains a *prd*-type homeodomain, four polyalanine tracts, an octapeptide and C-terminal (*aristaless*) domains (1,2). Located at Xp22.13, the *ARX* gene is considered to be a causative

*To whom correspondence should be addressed at: Department of Mental Retardation and Birth Defect Research, National Institute of Neuroscience, National Center of Neurology and Psychiatry, 4-1-1 Ogawahigashi, Kodaira, Tokyo 187-8502, Japan. Tel: +81 423461713; Fax: +81 423461743; Email: kitamura@ncnp.gp.jp or kuniokitamura@gmail.com
†The authors wish to be known that, in their opinion, they should be regarded to contribute equally to this work.
‡Present address: Department of Pediatrics, Graduate School of Medicine, University of Tokyo, Tokyo, Japan.

factor for X-linked lissencephaly and mental retardation (3–5), and more than 60 disease-related *ARX* mutations have been identified (6–8). These mutations are classified into two groups: one produces more severe lissencephaly and the other less severe mental retardation symptoms. The former group includes deletion, frameshift, nonsense and missense mutations within the homeobox and is associated with malformation syndromes such as lissencephaly, agenesis of the corpus callosum and ambiguous genitalia. The latter group includes elongation of the first or second polyalanine tract and missense mutations and is associated with syndromes without obvious malformations such as mental retardation, epilepsy and dystonia. The association of mental retardation with epilepsy is incidental since the patients sometimes had frequent and prolonged seizures, secondary neuronal injury and side effects of anticonvulsant. *ARX* mutations, however, provide a direct model for genetic association between epilepsy and mental retardation (9). Thus *ARX* is uniquely involved in a wide spectrum of neurodevelopmental disorders, ranging from mental retardation to lissencephaly.

Arx is expressed in the forebrain as well as in the testis, pancreas and skeletal muscles (3,10–12). It is involved in GABAergic neuron development in the cortex and striatum, in addition to cholinergic neuron development in the striatum, medial septum (MS) and ventral forebrain nuclei (3,13–15). Arx has both transcriptional activator and repressor domains (16) and functions as a transcriptional repressor (17). A portion of the genetic cascade of *Arx* in the forebrain has gradually been uncovered, with *Dlx2* and *Lmo1/Ebf3/Shox2* having recently been identified as upstream and target genes, respectively (18–20).

Important aspects to be addressed in the *ARX*-related syndromes, including lissencephaly and mental retardation, are (a) whether the single *ARX* mutations *per se* can cause one of the two syndromes and (b) whether there are specific causal relationships between individual *ARX* mutations and disease phenotypes. In the present report, we describe the generation of mice with three different knocked-in mutations associated with the *ARX*-related syndromes and show that the three mutations are causally involved in the syndromes and that the two mutations involved in the *ARX*-related mental retardation cause seizure and behavioral impairments through the abnormal development of GABAergic and cholinergic neurons.

RESULTS

Generation and general features of three *ARX* mutant mice

One of the mutations examined in this study was the mutation of a proline (353 in human ARX) in the conserved YPD (tyrosine–proline–aspartic acid) in the *prd*-type homeodomain of ARX. In humans, P353L develops X-linked myoclonic epilepsy with generalized spasticity and intellectual disability (OMIM300432), whereas P353R develops X-linked lissencephaly with ambiguous genitalia (XLAG, OMIM300215) (4,7). We also studied the addition of seven alanines to the first polyalanine tract, which leads to X-linked infantile spasms syndrome/West syndrome (OMIM308350) (4). We knocked-in the three mutations using homologous recombination; i.e. to study the first two mutations, we changed the equivalent proline (residue 355) of mouse Arx to either leucine or arginine, while seven GCG-triplets were inserted at residue 330 of the mouse *Arx* gene (Fig. 1A and B). Using Southern analysis of genomic DNA from embryonic stem (ES) cells, we confirmed that each mutation was correctly introduced into the *Arx* gene (Fig. 1C and D). Hemizygous mice ($Arx^{mt/Y}$) obtained by crossing female heterozygous mice ($Arx^{mt/X}$) with male wild-type mice ($Arx^{X/Y}$) were used in the subsequent experiments [$Arx^{mt/Y}$ mice: $Arx^{P355R/Y}$ (abbreviation: $Arx^{PR/Y}$), $Arx^{P355L/Y}$ ($Arx^{PL/Y}$), $Arx^{330ins(GCG)7/Y}$ ($Arx^{(GCG)7/Y}$) mice].

Arx protein from $Arx^{PR/Y}$ and $Arx^{PL/Y}$ embryos was the same length as that from the wild-type Arx, whereas the protein from $Arx^{(GCG)7/Y}$ embryos had a slightly higher molecular weight than that from the wild-type Arx owing to the addition of seven alanines (Fig. 1E). We examined the expression amounts of the mutated *Arx* transcripts and Arx proteins using quantitative real-time PCR and semi-quantitative western blotting, respectively. The amount of *Arx* transcript from $Arx^{PR/Y}$ embryos was approximately three times that of the wild-type *Arx* (this was also confirmed by the endpoint PCR, unpublished data), whereas those from $Arx^{PL/Y}$ and $Arx^{(GCG)7/Y}$ embryos were approximately equal to that of the wild-type *Arx* transcript (Fig. 1F). The amount of Arx protein in the $Arx^{PR/Y}$ embryo was approximately the same as in the wild-type Arx, whereas the protein from the $Arx^{PL/Y}$ and $Arx^{(GCG)7/Y}$ embryos was 40–60% that of the wild-type Arx; lower levels of protein were also found in another GCG mutant mouse, $Arx^{432\text{-}455dup/Y}$ (Fig. 1G, unpublished data). The low levels may be based on susceptibility to proteolysis of the mutated Arx, while detailed analysis of the mechanisms responsible for expression amounts of *Arx* transcript and protein in the $Arx^{PR/Y}$ embryo is required.

$Arx^{PR/Y}$ mice died within 1 day after birth, as did *Arx* deficient ($Arx^{-/Y}$) mice (3), whereas $Arx^{PL/Y}$ mice lived for more than 6 months. Most of the $Arx^{(GCG)7/Y}$ mice died within 3 months, but some of them survived for 5–6 months. Neonatal $Arx^{PR/Y}$ mice had smaller brains and olfactory bulbs, which were also seen in $Arx^{-/Y}$ mice (3), whereas the neonatal brains of $Arx^{PL/Y}$ and $Arx^{(GCG)7/Y}$ mice were nearly as large as those of $Arx^{X/Y}$ mice (Fig. 1H).

Disturbed development of GABAergic and cholinergic neurons in embryonic and neonatal $Arx^{PR/Y}$, $Arx^{PL/Y}$ and $Arx^{(GCG)7/Y}$ mice

Arx deficiency results in the loss of most of the tangential migration, except for that along the subventricular zone (3). The migration of GABAergic progenitor cells was examined using mutant mice cross-bred with heterozygous glutamate decarboxylase (GAD) 67-GFP (Δneo) mice, ($GAD67^{GFP/+}$ mice) (21,22), which demonstrated that most of the GABAergic interneuron precursors expressed Arx (Fig. 2A–D). The migration modes in $Arx^{PR/Y}$ and $Arx^{PL/Y}$ embryos were very different from one another (Fig. 2B and C). Arx^{+} GABAergic progenitor cells of $Arx^{PR/Y}$ embryos failed to initiate migration at E12.5 (Fig. 2B) and began to migrate only along the subventricular zone of the cortex at E14.5 (inset of Fig. 2B). The total number of Arx^{+} cells was 28.5 ± 3.4%

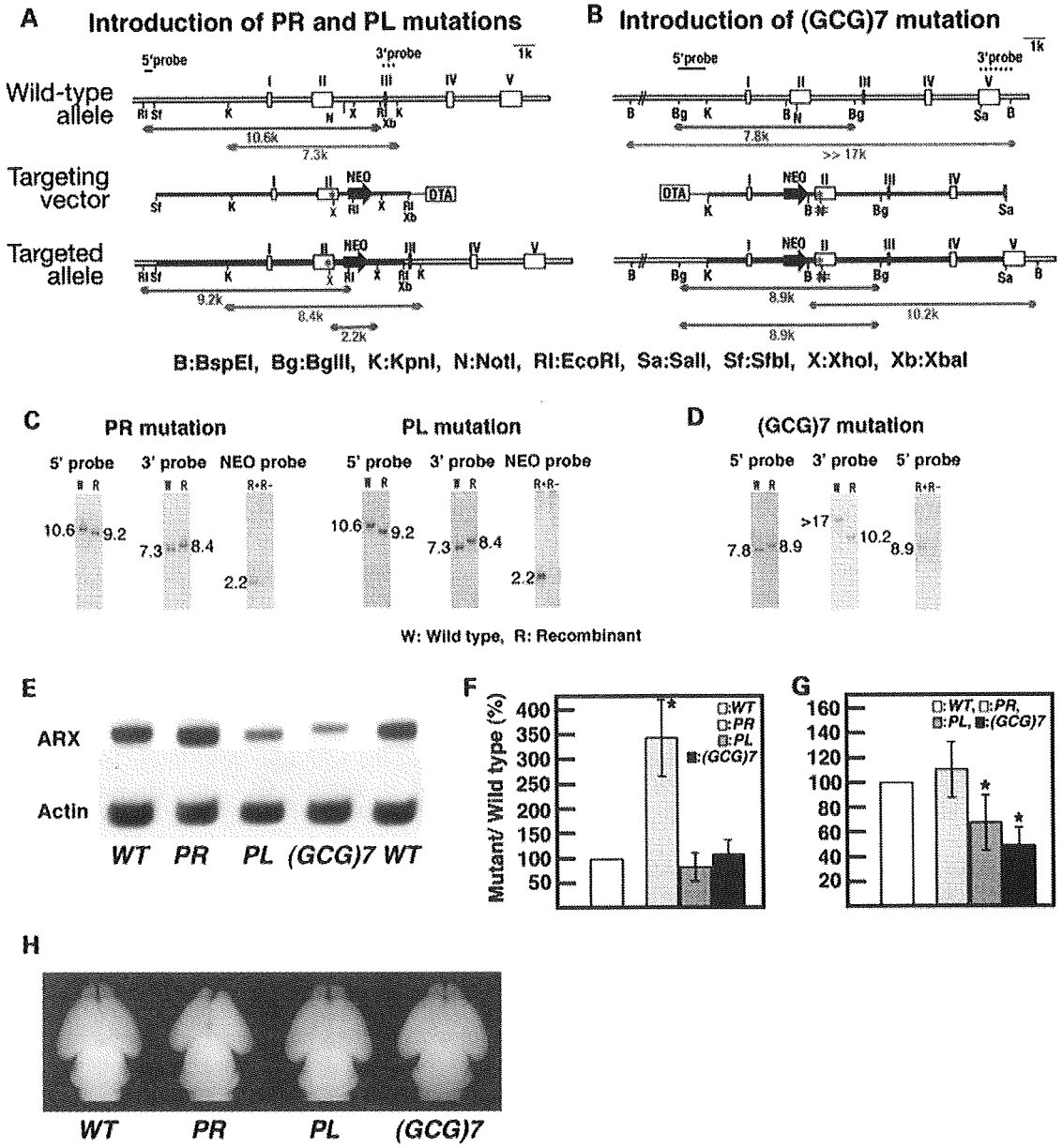

Figure 1. Generation and general features of $Arx^{PR/Y}$, $Arx^{PL/Y}$ and $Arx^{(GCG)7/Y}$ mice. (**A** and **B**) Schematic representation of the wild-type *Arx* allele (top), targeting vector (middle) for introducing either the PL or PR mutations (A) and the (GCG)7 mutation (B), and the mutated allele after homologous recombination (bottom). The mutation points are indicated by (*). A new *Xho*I site is formed upon the introduction of the PL or PR mutations (A), whereas a *Not*I site is destroyed upon the introduction of the (GCG)7 mutation (B). (**C** and **D**) Southern blot analysis of the targeted ES clone with either the PL or PR mutations (C) and the (GCG)7 mutation (D). Genomic DNA from the ES cells was digested with either *Eco*RI for the PL/PR mutations (red bar in A) or *Bgl*II for the (GCG)7 mutation (red bar in B), and both digests were probed with a 5′-probe (C and D). Genomic DNA was then digested with *Kpn*I for the PL/PR mutations (blue bar in A) or *Bam*HI for the (GCG)7 mutation (blue bar in B), and both digests were probed with a 3′-probe (C and D). To confirm that each mutation was introduced, genomic DNA was either digested with *Xho*I (green line in A) and probed with a Neo-probe for the PL/PR mutations (C) or digested with *Bgl*II/*Not*I (green bar in B) and probed with a 5′-probe for the (GCG)7 mutation (D). (**E**) Western blotting of Arx protein from the forebrains of three mutant embryos at E14. Arx protein from $Arx^{PR/Y}$ and $Arx^{PL/Y}$ embryos was the same length as the wild-type Arx, whereas the protein from $Arx^{(GCG)7/Y}$ embryos had a slightly higher molecular weight than that from the wild-type Arx. (**F**) Quantitative analysis of *Arx* transcript by real-time PCR. All values of the *Arx* transcript were normalized for *Gapdh*. The *Arx* transcript from $Arx^{PR/Y}$ embryos was approximately three times that of the wild-type *Arx*, whereas the *Arx* transcripts of $Arx^{PL/Y}$ and $Arx^{(GCG)7/Y}$ embryos were approximately the same as those of the wild-type *Arx*. (**G**) Semi-quantitative analysis of Arx protein by western blotting. All values of the Arx protein were normalized for actin. Arx protein levels from $Arx^{PR/Y}$ embryos were approximately the same as those from the wild-type Arx, whereas Arx protein levels in $Arx^{PL/Y}$ and $Arx^{(GCG)7/Y}$ embryos were 66.4 ± 22.6% ($P < 0.02$, $n = 5$) and 48.4 ± 16.4% ($P < 0.001$, $n = 5$) of those in the wild-type Arx, respectively. (**H**) Dorsal views of whole brains of newborn mice. $Arx^{PR/Y}$ mice had smaller brains and olfactory bulbs, whereas the neonatal brains of $Arx^{PL/Y}$ and $Arx^{(GCG)7/Y}$ mice were almost as large as those of $Arx^{X/Y}$ mice.

($P < 0.001$, $n = 3$) of that found in wild-type cells in the cortical plate at P0 (Fig. 2F). The Arx^{+} GABAergic progenitor cells of $Arx^{PL/Y}$ and $Arx^{(GCG)7/Y}$ embryos began to migrate at E12.5 (Fig. 2C and D), finally reaching 92.8 ± 8.7% and 88.4 ± 11.2% ($P < 0.02$, $n = 3$), respectively, of the number of wild-type cells found in the cortical plate at P0 (Fig. 2G

and H). Thus, the PR mutation associated with XLAG resulted in severe defects in cortical tangential migration from the medial ganglionic eminence (MGE), whereas the PL and (GCG)7 mutations associated with *ARX*-related mental retardation resulted in only slight impairments.

Arx deficiency results in a thickened subventricular zone of striatum and a loss of GABAergic interneurons in the striatum, suggesting the inhibition of both the radial migration of GABAergic projection neurons from the lateral ganglionic eminence and the tangential migration of GABAergic interneurons from the MGE (3,15). Arx^{+} and $MAP2^{-}$ ventricular and subventricular zones of the striatum were thicker in the $Arx^{PR/Y}$ mice at P0 (asterisk in Fig. 2J1 and J2). Furthermore, somatostatin $(SST)^{+}$ cells, a subtype of GABAergic interneurons, accumulated in the subventricular zone of the ventral striatum (around the nucleus accumbens), but no SST^{+} cells were detected in the mantle zone of the striatum (Fig. 2N). Thus, both radial and tangential migrations were significantly suppressed in the $Arx^{PR/Y}$ mice, and a very similar situation was seen with the $Arx^{-/Y}$ mice (3,15). Radial migration in the $Arx^{PL/Y}$ and $Arx^{(GCG)7/Y}$ mice, on the other hand, was barely suppressed compared with that in the $Arx^{PR/Y}$ mice at P0 (Fig. 2K1, K2, L1, L2), whereas tangential migration of striatal SST^{+} cells was suppressed in a manner dependent on each mutation (Fig. 2O and P). Thus, the PR mutation induced severe defects in striatum formation, which depends on both the radial and tangential migrations of presumptive GABAergic neurons, whereas the PL and (GCG)7 mutations caused impairments only in tangential migration of interneurons to the striatum.

Arx induces Gbx1 and Lhx8, making it essential for the development of cholinergic neurons; no cholinergic neurons were detected in the forebrain of the $Arx^{-/Y}$ mice (15). In $Arx^{PR/Y}$ and $Arx^{(GCG)7/Y}$ mice, no *Lhx8* expression was found in the striatum at P0 (Fig. 2R and T), and only a slight reduction in *Lhx8* expression was detected in the striatum of $Arx^{PL/Y}$ mice (Fig. 2S). ARX was expressed in the MS and the vertical limbs of the nucleus of the diagonal bands (DBv) of $Arx^{X/Y}$ mice at P0 (Fig. 2U), whereas no expression was seen in $Arx^{PR/Y}$ mice (Fig. 2V). Furthermore, the $Arx^{PL/Y}$ and $Arx^{(GCG)7/Y}$ mice showed much reduced ARX expression in the MS and DBv (Fig. 2W and X). These Arx expression patterns in the MS and DBv of the three mutants were also seen for *Lhx8* expression (data not shown).

$Arx^{-/Y}$ mice with a nonsense mutation that causes XLAG show a thinner cortical plate without a severely abnormal structure (such as inversion of cortical layers) at P0 (3). $Arx^{PR/Y}$ mice with the missense mutation that causes XLAG also exhibited a thinner cortical plate compared with $Arx^{X/Y}$ mice at P0 ($85.2 \pm 4.8\%$ of wild-type, $P < 0.01$, $n = 3$. Fig. 3A and B) The ratio of $Tbr1^{+}$ deep layer (23) to whole cortical plate in $Arx^{PR/Y}$ mice was slightly higher than that of the wild-type (Fig. 3G and H), whereas the $Foxp1^{+}$ middle layer (24), located at the upper side of the cortical plate, exhibited no clear middle layer structure compared with wild-type (Fig. 3E and F). Furthermore, the $Satb2^{+}$ cells (25) were packed together in the uppermost layer, resulting in a thinner $Satb2^{+}$ upper layer (Fig. 3C and D). Thus, the abnormal cortical structure in $Arx^{PR/Y}$ mice at P0 suggests that fine regulation in both the proliferation of neuroepithelial cells in the ventricular zone (3) and the inside-out migration of post-mitotic neurons may be perturbed by $Arx^{PR/Y}$ protein expression in the embryonic ventricular/subventricular zones. Furthermore, this perturbation may be one reason why three cortical layers are formed in the human cortex with XLAG (26,27). No thin cortical plate or abnormal layer structure was observed in the $Arx^{PL/Y}$ and $Arx^{(GCG)7/Y}$ mice containing mutations that cause mental retardation (data not shown).

The addition of seven alanines to the first polyalanine tract of Arx *in vitro* results in the formation of intranuclear inclusions and increased apoptosis (28,29), whereas the present *in vivo* study using $Arx^{(GCG)7/Y}$ embryos showed that no specific formation of intranuclear inclusions occurs in the migratory Arx^{+} cells from ganglionic eminence at E12 and in the cortical Arx^{+} cells at P0 (Supplementary Material, Fig. S1A–D). Furthermore, no increased apoptosis was detected in the ganglionic eminence at E12 (Supplementary Material, Fig. S1E and F). These observations were also seen in another mutation type in the GCG tracts, the duplication of polyalanine tract, '432–455dup' (unpublished data). The absence of intranuclear inclusions in the present *in vivo* study could be based on differences in the *in vivo* and *in vitro* solubility/stability of Arx protein with extra alanine tracts.

In summary, the phenotype of mice with the PR mutation was entirely different from that of mice with the PL and (GCG)7 mutations; this strongly suggests that both groups of mutations can cause specifically developmental abnormalities in *ARX*-related lissencephaly (XLAG) or mental retardation. In order to further understand mutation effects on *ARX*-related mental retardation, we focused on the seizure, behavioral and neuronal analysis of the $Arx^{PL/Y}$ and $Arx^{(GCG)7/Y}$ mice at the post-natal stage.

Epilepsy in the $Arx^{PL/Y}$ and $Arx^{(GCG)7/Y}$ mice

Epilepsy is a common symptom in *ARX*-related mental retardation, and we examined the presentation of the epilepsy in both the types of mice. In the behavioral monitoring experiment, seizures were noted in 70% (7/10) of the $Arx^{(GCG)7/Y}$ mice at P1m (1-month-old mice), and one of them (1/10) died during status epilepticus. All seizures started with trembling of the limbs and progressed to tonic clonic convulsions, running fits and then complete loss of postural control and movement (Supplementary Material, Movie). Some of the mice exhibited hand-washing motions at the end of the seizures. Histologically, ectopically induced NPY expression in mossy fibers of the dentate gyrus was found in the brains of $Arx^{(GCG)7/Y}$ mice presenting seizures (Fig. 4A1 and A2).

In three pairs of $Arx^{(GCG)7/Y}$ mice and their wild-type littermates, electroencephalographics (EEGs) were recorded in the frontal cortex, hippocampus and striatum together with the behavioral monitoring (Fig. 4B1 and B2). In all three $Arx^{(GCG)7/Y}$ mice, the ictal EEG showed abnormal activities, although no spikes were found during the interictal period (Fig. 4C). At the beginning of the seizure, EEG showed positive spikes in the hippocampus and negative spikes in the frontal cortex and striatum, followed by diffuse spike bursts (Fig. 4D). The first spikes in 26 of 29 seizures were seen simultaneously in the hippocampus, frontal cortex and striatum.

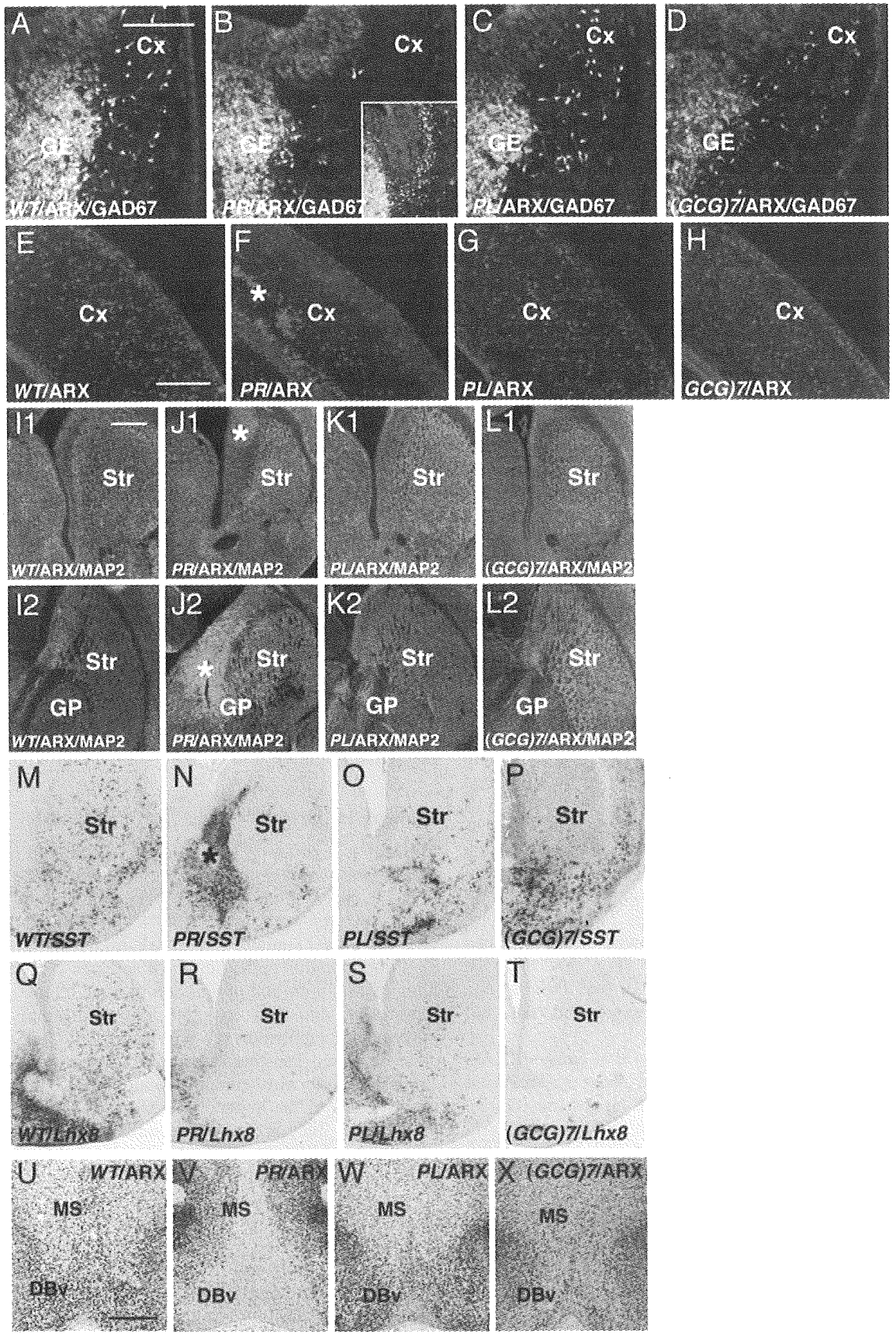
A
Cx
GE
WT/ARX/GAD67
B
Cx
GE
PR/ARX/GAD67
C
Cx
GE
PL/ARX/GAD67
D
Cx
GE
(GCG)7/ARX/GAD67
E
Cx
WT/ARX
F
*
Cx
PR/ARX
G
Cx
PL/ARX
H
Cx
GCG)7/ARX
I1
Str
WT/ARX/MAP2
J1
*
Str
PR/ARX/MAP2
K1
Str
PL/ARX/MAP2
L1
Str
(GCG)7/ARX/MAP2
I2
Str
GP
WT/ARX/MAP2
J2
*
Str
GP
PR/ARX/MAP2
K2
Str
GP
PL/ARX/MAP2
L2
Str
GP
(GCG)7/ARX/MAP2
M
Str
WT/SST
N
*
Str
PR/SST
O
Str
PL/SST
P
Str
(GCG)7/SST
Q
Str
WT/Lhx8
R
Str
PR/Lhx8
S
Str
PL/Lhx8
T
Str
(GCG)7/Lhx8
U
WT/ARX
MS
DBv
V
PR/ARX
MS
DBv
W
PL/ARX
MS
DBv
X
(GCG)7/ARX
MS
DBv

Then 20–30 Hz spike bursts with waxing and waning appeared in the hippocampus, and there were continuous bursts of very high-voltage spikes in the striatum. Finally, the bursts abruptly changed to long-lasting, low-voltage activity with synchronous rhythmic theta waves. Seizures often occurred in clusters, and the spikes were found between the seizure clusters.

In contrast, no $Arx^{PL/Y}$ mice died during the behavioral monitoring. Only one tonic seizure was seen at P1m in the $Arx^{PL/Y}$ mice (1/10), and the seizure was of shorter duration (30 s) than those seen in the $Arx^{(GCG)7/Y}$ mice (146 ± 57.9 s), but no seizures were observed in $Arx^{PL/Y}$ mice during EEG recordings. To determine the threshold of seizure and the relationship between age and seizure, the $Arx^{PL/Y}$ and $Arx^{X/Y}$ mice were challenged with bicuculline, a $GABA_A$ receptor inhibitor, at P1 m and P3–5m at a relatively low dosage (1.5 mg/kg). Myoclonic jerks were observed in most of the mice with both genotypes at both P1m and P3–5m, whereas generalized seizures developed less frequently in the $Arx^{X/Y}$ mice at P3–5m [Table 1(A)]. Furthermore, significant differences were noted in the time from injection to onset of jerks and generalized seizures as well as in the number of deaths at both P1m and P3–5m [Table 1(A) and (B)]. Thus, the seizure threshold was significantly lower in the $Arx^{PL/Y}$ mice than in the control $Arx^{X/Y}$ mice.

Impaired learning performance in both the $Arx^{PL/Y}$ and $Arx^{(GCG)7/Y}$ mice

Learning and memory of both types of mice were tested using a step-through passive avoidance task and two tasks on the eight-arm radial maze. A step-through passive avoidance task determines whether mice can retain an aversive memory of electric shocks. Naïve $Arx^{PL/Y}$ and $Arx^{(GCG)7/Y}$ mice showed no significant difference in latency to enter a darkened chamber compared with $Arx^{X/Y}$ mice ($P = 0.098$ and $P = 0.792$, respectively, Mann–Whitney's U-test), which indicated that mobility and motivation for entry were not affected (Fig. 5A and B). After the mice had experienced shocks, latency for entry was significantly shorter in both $Arx^{PL/Y}$ and $Arx^{(GCG)7/Y}$ mice than in $Arx^{X/Y}$ mice ($P = 0.021$ and $P < 0.001$, respectively, Mann–Whitney's U-test), with a greater reduction of latency seen in $Arx^{(GCG)7/Y}$ mice (Fig. 5A and B). These results indicated that neither type of mutant mouse could successfully acquire avoidance behavior through aversive experience.

The win-shift task on the eight-arm radial maze is a well-known hippocampus-dependent spatial learning task. To efficiently obtain all eight pellets at the end of each arm, mice must retain the spatial locations of pellet-retrieved arms within a trial. Performance was evaluated for accuracy, measured as the percentage of chosen arms that were baited. $Arx^{PL/Y}$ mice showed significantly improved accuracy with training, but their accuracy was slightly lower than that of $Arx^{X/Y}$ mice (genotype effect, $F[1,17] = 9.12$, $P < 0.01$; training effect, $F[5,85] = 33.1$, $P < 0.0001$; genotype × training interaction, $F[5,85] = 0.702$, $P = 0.624$) (Fig. 5C). In $Arx^{(GCG)7/Y}$ mice, the accuracy was significantly poorer than in $Arx^{X/Y}$ mice (genotype effect, $F[1,17] = 84.3$, $P < 0.0001$; genotype × training interaction, $F[3,51] = 10.8$, $P < 0.0001$), as the $Arx^{(GCG)7/Y}$ mice showed no significant improvement in accuracy with training ($F[3,18] = 0.302$, $P = 0.824$, one-way RMANOVA) (Fig. 5D). These results indicate that both mutants showed inaccurate performance in pellet retrieval, with the $Arx^{(GCG)7/Y}$ mice showing more severe impairment than the $Arx^{PL/Y}$ mice. Because neither mutant used a non-spatial egocentric strategy by visiting each of the eight arms in turn (Supplementary Material, Fig. S2), disabled spatial learning was thought to underlie the inaccurate performance of each type.

The win-stay task of the eight-arm radial maze is designed to evaluate striatum-dependent procedural learning in rodents. Mice can obtain a reward whenever they approach a lit arm. The arrangement of four lit arms is changed for every trial to avoid interfering with spatial memory. After acquiring a manner of approaching lit arms, mice approach the unlit arms less frequently. $Arx^{PL/Y}$ mice showed no significant difference in the ratio of unlit arm choices to lit arm choices compared with the $Arx^{X/Y}$ mice (genotype effect, $F[1,22] = 1.78$, $P = 0.20$; genotype × training interaction, $F[7,154] = 0.43$, $P = 0.88$) (Fig. 5E). In contrast, $Arx^{(GCG)7/Y}$ mice showed a significantly higher unlit-to-lit ratio throughout training than the $Arx^{X/Y}$ mice did, although they did show a significantly decreased ratio with training (genotype effect, $F[1,9] = 31.2$, $P < 0.001$; training effect, $F[4,36] = 13.4$, $P < 0.001$; genotype × training interaction, $F[4,36] = 0.19$, $P = 0.94$) (Fig. 5F). Thus, we concluded that the $Arx^{(GCG)7/}$

Figure 2. Characterization of the cortex (Cx), striatum (Str) and medial septum (MS) of embryonic and neonatal $Arx^{PR/Y}$, $Arx^{PL/Y}$ and $Arx^{(GCG)7/Y}$ mice. (**A–D**) Cortical tangential migration in embryos (E12.5) crossbred with GAD67 $^{GFP/+}$ mice. Arx^+ (red)/GAD67-GFP^+ (green) cells in the $Arx^{X/Y}$ embryos began to migrate from the ganglionic eminence (GE) (A), whereas no migration from the GE was seen in the $Arx^{PR/Y}$ embryos (B). Only late migration from the GE along the subventricular zone of the Cx was seen at E14.5 (inset of B). Arx^+/GAD67-GFP^+ cells in $Arx^{PL/Y}$ and $Arx^{(GCG)7/Y}$ embryos migrated normally, although the number of cells was slightly reduced compared with that in the $Arx^{X/Y}$ embryos (C, D). (**E–H**) Arx^+ cells in the Cx at P0 (E–H). Significantly reduced numbers of Arx^+ cells were seen in the $Arx^{PR/Y}$ mice, and some of them were clustered at the subplate (F). Arx^+ cells were only slightly reduced in the $Arx^{PL/Y}$ and $Arx^{(GCG)7/Y}$ mice (G, H). (**I1–L1**) Anterior Str and (**I2–L2**) posterior Str, ARX (red) and MAP2 (green) expression in the Str at P0. The Arx^+ and $MAP2^-$ ventricular zone of the anterior Str of $Arx^{PR/Y}$ mice showed increased thickness (* in J1), whereas no increase was seen in $Arx^{PL/Y}$ (K1) or $Arx^{(GCG)7/Y}$ mice (L1). The thickening of the ARX^+ and $MAP2^+$ ventricular zone was also seen in the posterior Str of $Arx^{PR/Y}$ mice (* in J2), whereas no increase was seen in the $Arx^{PL/Y}$ (K2) and $Arx^{(GCG)7/Y}$ mice (L2). (**M–P**) SST^+ interneurons in the Str at P0. SST^+ interneurons were distributed throughout the Str of the $Arx^{X/Y}$ mice (M), whereas they gathered in the thickened ventricular zone of the striatum of $Arx^{PR/Y}$ mice (* in N) and were not present in the mantle zone of the Str (N). On the other hand, a small number of SST^+ interneurons were seen in the mantle zone of the Str of $Arx^{PL/Y}$ mice compared with $Arx^{X/Y}$ mice (O), whereas most of the SST^+ interneurons were seen in the ventricular zone of the Str in $Arx^{(GCG)7/Y}$ mice (P). (**Q–T**) *Lhx8* expression in the Str at P0. *Lhx8* expression was seen throughout the Str of $Arx^{X/Y}$ mice (Q), whereas no expression was seen in $Arx^{PR/Y}$ mice (R). *Lhx8* expression was seen in the ventral half of the Str of $Arx^{PL/Y}$ mice (S), whereas no expression was seen in the $Arx^{(GCG)7/Y}$ mice (T). (**U–X**) Arx expression in the MS and vertical limbs of the nucleus of the diagonal band (DBv) at P0. ARX was expressed in the MS and DBv of the $Arx^{X/Y}$ mice (U), but no expression was seen in $Arx^{PR/Y}$ mice (V). Furthermore, significantly reduced Arx expression was observed in the $Arx^{PL/Y}$ and $Arx^{(GCG)7/Y}$ mice (W, X). MGE: medial ganglionic eminence, GP: globus pallidus. Scale bars: A–D, 100 μm; E–H, 250 μm; I1–T, 500 μm; U–X, 500 μm.

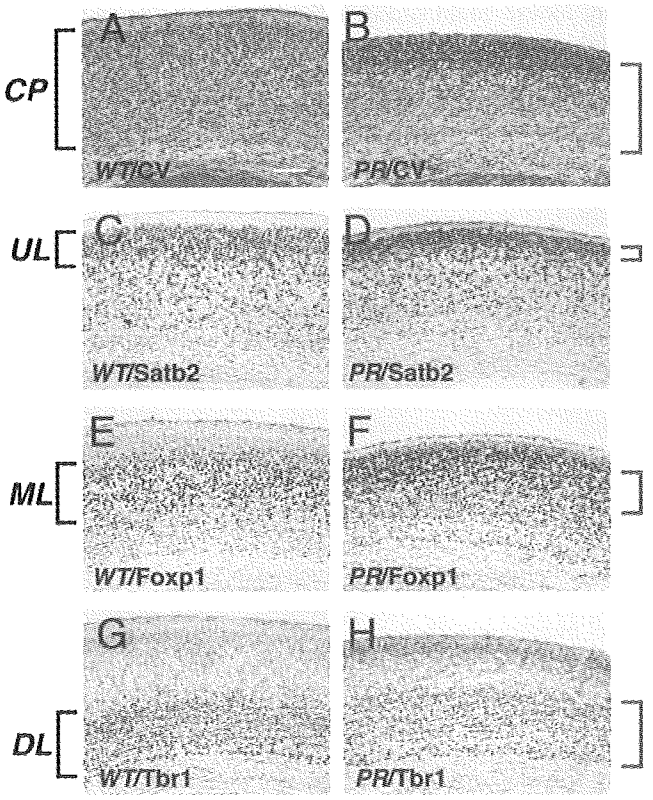

Figure 3. Aberrant cortical layer formation in $Arx^{PR/Y}$ mice. (**A** and **B**) Cresyl violet staining of the cortical plate of $Arx^{X/Y}$ (A) and $Arx^{PR/Y}$ (B) mice at P0. The thickness of the cortical plate was 85.2 ± 4.8% of wild-type ($P < 0.01$, $n = 3$). (**C** and **D**) Satb2 imaging of the upper cortical layer of $Arx^{X/Y}$ (C) and $Arx^{PR/Y}$ (D) mice. Satb2$^+$ cells in $Arx^{PR/Y}$ mice were packed together in the uppermost layer, resulting in a thinner Satb2$^+$ upper layer than that of the wild-type. (**E** and **F**) Foxp1 imaging of the middle cortical layer of $Arx^{X/Y}$ (E) and $Arx^{PR/Y}$ (F) mice. The Foxp1$^+$ middle layer of $Arx^{PR/Y}$ mice was located at the upper side of the cortical plate and exhibited no clear middle layer structure compared to wild-type. (**G** and **H**) Tbr1 imaging of the deep cortical layer of $Arx^{X/Y}$ (G) and $Arx^{PR/Y}$ (H) mice. The ratio of the Tbr1$^+$ deep layer to the entire cortical plate in $Arx^{PR/Y}$ mice (60.3 ± 5.3%, $P < 0.01$, $n = 3$) was slightly higher than that of $Arx^{X/Y}$ mice (48.3 ± 3.8%, $P < 0.01$, $n = 3$). CP, cortical plate; UL, upper layer; ML, middle layer; DL, down layer. Scale bars: A–H, 100 μm.

^{Y} mice failed to acquire an association between the stimulus of light and the response of approaching, indicating a deficit in procedural learning.

In addition to several kinds of learning disabilities, we confirmed the impaired motor coordination in Arx^{PL} and $Arx^{(GCG)7/Y}$ mice and the increased locomotor activity and anxiety-like behavior in $Arx^{(GCG)7/Y}$ mice (Supplementary Material, Figs S3 and S4). Increased locomotor activity and anxiety-like behavior are thought to affect learning indices; however, the above-mentioned results in learning tasks were statistically independent from the increased locomotor activity and anxiety-like behavior in $Arx^{(GCG)7/Y}$ mice (Supplementary Material, Table S1).

Slight and severe reduction of GABAergic neurons in the cortex and striatum, respectively, of $Arx^{PL/Y}$ and $Arx^{(GCG)7/Y}$ mice at P1m

We examined the post-natal distribution of GABAergic and cholinergic neurons based on the occurrence of seizure and impaired learning performance. In addition to being expressed during the embryonic period, Arx is expressed in each subtype of GABAergic interneurons, such as the parvalbumin (PV)$^+$, SST$^+$ and neuropeptide Y (NPY)$^+$ cells and choline acetyltransferase (ChAT)$^+$ cholinergic neurons in the post-natal period (Supplementary Material, Fig. S5). Furthermore, the findings at P1m described in this and the following sections were also confirmed at P2m (data not shown); thus, they were not due merely to a developmental delay.

We examined the number of GAD67$^+$ neurons and subtypes of GABAergic interneurons in the somatosensory cortex of $Arx^{PL/Y}$ and $Arx^{(GCG)7/Y}$ mice at P1m. GAD67$^+$, SST$^+$, NPY$^+$ and PV$^+$ interneurons exhibited no severe reduction in the cortex of $Arx^{PL/Y}$ and $Arx^{(GCG)7/Y}$ mice, with some exceptions, as suggested by the tangential migration of Arx$^+$ GABAergic neurons during the embryonic and neonatal stages (Supplementary Material, Fig. S6, Fig. 2C, D, G, H). Tangential migration of striatal SST$^+$ cells was suppressed in a manner dependent on each mutation at P0 (Fig. 2O and P). This observation suggested that these subtypes may be reduced at post-natal stages and there were clearly fewer SST$^+$, NPY$^+$ and NOS (NO synthase)$^+$ interneurons in the striatum of the $Arx^{PL/Y}$ and $Arx^{(GCG)7/Y}$ mice (Fig. 6A–I, M). On the other hand, there was only a slight reduction in the number of PV$^+$ interneurons in both mutants when compared with the other subtypes (Fig. 6J–L, M). Furthermore, we found that SST$^+$, NPY$^+$ and NOS$^+$ interneurons were localized to the ventral region and were rarely detected in the dorsal region of the striatum, whereas no regional differences were seen for PV$^+$ interneurons (Fig. 6A–L). Thus, the number of SST$^+$, NPY$^+$ and NOS$^+$ interneurons in the striatum of both mutants was significantly reduced when compared with that seen in the cortex, suggesting that striatal tangential migration was specifically suppressed in both mutants. We also found a subtype-specific reduction in the GABAergic interneurons in the basolateral amygdala of both mutants (Supplementary Material, Fig. S7).

Figure 4. Presentation of seizures in $Arx^{(GCG)7/Y}$ mice. (**A1** and **A2**) Ectopic NPY expression in mossy fibers of the dentate gyrus. Before seizure (A1), after seizure (A2). (**B1** and **B2**) Diagrams of the electrode configuration superimposed on a coronal section of the brain. Local EEG was simultaneously recorded from the striatum (B1) and hippocampus (B2), together with the ipsilateral frontal EEG (B1). The recording sites were histologically verified in the cresyl violet staining sections. (**C**) Ictal EEG activity in three $Arx^{(GCG)7/Y}$ mice (#1, #2, #3). The seizure started (dotted line) simultaneously in the hippocampus, frontal cortex and striatum, followed by diffuse spike bursts. Next, 20–30 Hz spike bursts with waxing and waning appeared in the hippocampus (bar). Then there were continuous bursts of very high-voltage spikes (open bar) in the striatum, which abruptly changed into a long-lasting low-voltage activity with synchronous rhythmic theta waves. All seizures started with limb trembling that progressed to tonic clonic seizures (closed triangle), running fits (arrow) and complete loss of postural control and movement (open arrow). (**D**) Examples of EEG data at the beginning of a seizure in three $Arx^{(GCG)7/Y}$ mice (#1, #2, #3). The first spikes are simultaneously seen in the frontal cortex, hippocampus and striatum. F-cx, frontal cortex; Hip, hippocampus; Str-l, lower electrode in the striatum; Str-u, upper electrode in the striatum; Str-BP, bipolar in the striatum.

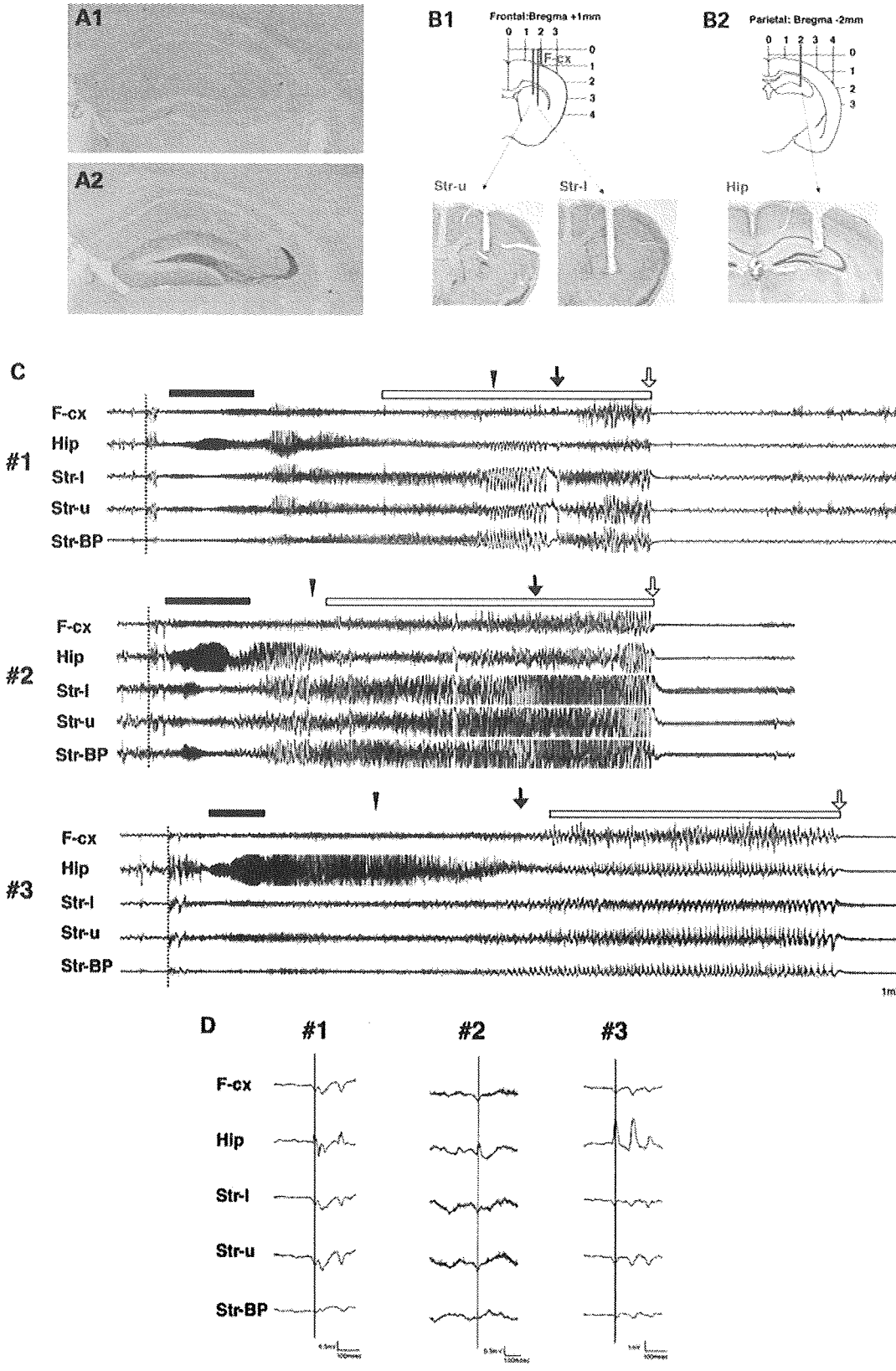
A1
A2
B1
Frontal:Bregma +1mm
0 1 2 3
F-cx
0
1
2
3
4
Str-u
Str-l
B2
Parietal: Bregma -2mm
0 1 2 3 4
0
1
2
3
Hip
C
#1
F-cx
Hip
Str-l
Str-u
Str-BP
#2
F-cx
Hip
Str-l
Str-u
Str-BP
#3
F-cx
Hip
Str-l
Str-u
Str-BP
1mV
2sec
D
#1
#2
#3
F-cx
Hip
Str-l
Str-u
Str-BP

Table 1. Seizure induction by bicuculline in $Arx^{PL/Y}$ mice

(A) The number of mice displaying myoclonic jerks and generalized seizures and of deaths in the $Arx^{PL/Y}$ and $Arx^{X/Y}$ mice

Post-natal month old	Genotype	Mice with myoclonic jerks/total	Mice with generalized seizure/total	Deaths/total
P1m	$Arx^{P355L/Y}$	6/6	6/6	6/6
P3–5m	$Arx^{X/Y}$	6/6	4/6	1/6
	P	1	0.4546	0.0152*
P3–5m	$Arx^{P355L/Y}$	8/8	8/8	8/8
	$Arx^{X/Y}$	7/8	3/8	2/8
	P	1	0.0256*	0.0070**

(B) The onset of myoclonic jerks, generalized seizures and death from injection in the $Arx^{PL/Y}$ and $Arx^{X/Y}$ mice

Post-natal month old	Genotype	Time myoclonic jerks start (min)	Time generalized seizure start (min)	Time of death (min)
P1m	$Arx^{P355L/Y}$	2.82 ± 0.60	3.58 ± 0.97	17.00 ± 9.69
	$Arx^{X/Y}$	5.43 ± 0.81	6.97 ± 1.83	18.00 ± 0
	P	0.0039**	0.0105*	
P3–5m	$Arx^{P355L/Y}$	3.34 ± 0.51	4.54 ± 1.62	9.00 ± 1.69
	$Arx^{X/Y}$	6.57 ± 4.16	9.53 ± 5.17	15.25 ± 1.06
	P	0.0038**	0.0143*	

Values are mean ± SD.
*$P < 0.05$.
**$P < 0.01$.

Reduction of cholinergic neurons in the striatum, MS and ventral forebrain nuclei of $Arx^{PL/Y}$ and $Arx^{(GCG)7/Y}$ mice at P1m

Striatal ChAT$^+$ cholinergic interneurons were reduced by 50.1 ± 6.8% ($P < 0.001$, n=3) in the $Arx^{PL/Y}$ mice, whereas no ChAT$^+$ interneurons were found in the $Arx^{(GCG)7/Y}$ mice, as expected from the *Lhx8* expression at P0 (Figs 2S, T and 7B, C). $Arx^{432\text{-}455dup/Y}$ mice also had no ChAT$^+$ interneurons in the striatum (unpublished data). This observation suggests that migration and differentiation of cholinergic interneurons are fully suppressed by the elongation of the first and second polyalanine tracts and only partially by the PL mutation.

Forebrain cholinergic projection neurons are found in the MS (Ch1), DBv and DBh (Ch2 and Ch3) and the basal magnocellular complex (Ch4), which is composed of the magnocellular preoptic nucleus (MCPO), substantia innominata, ventral pallidum and basal nucleus (NB). Ch1 and Ch2 provide major innervation to the hippocampus; Ch3 innervates the olfactory bulb and Ch4 innervates the cortex. ChAT$^+$ projection neurons were significantly reduced, to 53.2 ± 4.8% of the wild-type level in the MS of the $Arx^{PL/Y}$ mice ($P < 0.001$, $n = 3$, Fig. 7E), and were even more severely reduced in the $Arx^{(GCG)7/Y}$ mice (23.8 ± 4.0%, $P < 0.001$, $n = 3$, Fig. 7F). Furthermore, the ChAT$^+$ neurons of $Arx^{PL/Y}$ and $Arx^{(GCG)7/Y}$ mice were reduced more severely in the DBv than in the MS (Fig. 7E, F). GAD67$^+$ neurons, another component of both the MS and DBv, were reduced in the $Arx^{PL/Y}$ mice and were not found in the $Arx^{(GCG)7/Y}$ mice, except for some expression in the most anterior MS and DBv (Fig. 7H, I and inset of I). The number of ChAT$^+$ neurons in the MCPO of both mutants was decreased to ~70% of the wild-type level (80.1 ± 8.5%, $P < 0.01$, $n = 3$ for $Arx^{PL/Y}$ mice, 68.4 ± 7.5%, $P < 0.001$, $n = 3$ for $Arx^{(GCG)7/Y}$ mice, Fig. 7J–L), and the number of neurons in the NB of both mutants was also reduced (data not shown). Furthermore, we detected acetylcholinesterase (AchE)$^+$ axonal arbors of cholinergic projection neurons in the hippocampus and cortex, which are innervated by cholinergic projection neurons in the MS and basal magnocellular complex, respectively. A clear reduction in the AchE$^+$ axonal arbors was noted in the hippocampus and somatosensory cortex of $Arx^{PL/Y}$ mice (Fig. 7N, Q, S) compared with $Arx^{X/Y}$ mice, in addition to a severe reduction seen in $Arx^{(GCG)7/Y}$ mice (Fig. 7O, R, S). These data indicate aberrant formation of the Ch1/Ch2 (septohippocampal) and C4 systems in both mutant strains.

DISCUSSION

Diversity of *ARX* mutations and XLAG and mental retardation with epilepsy

One question to be addressed regarding the diversity of *ARX* mutations in the XLAG and mental retardation is whether the conditions are caused by individual mutations without involvement of any other genetic factors. We addressed this topic by introducing PR, PL and (GCG)7 mutations into the mouse genome. We found that phenotypes of $Arx^{PR/Y}$ mice are very similar to those of $Arx^{-/Y}$ mice with a truncated *ARX* mutation in XLAG (3,15). The abnormal cortical layer formation, abnormal structure of the striatum and deficiency of GABAergic neurons in the cortex and striatum caused by PR mutation closely mimic XLAG (5,26,27). Still, the mechanisms underlying the abnormal cortical formation specific to XLAG are not yet clear due to the perinatal death of both mouse models of XLAG (30,31). On the other hand, two structurally different mutations associated with *ARX*-related mental retardation, including the single amino acid replacement (PL) and elongation of polyalanine tract [(GCG)7], also caused a common phenotype of *ARX*-related mental retardation with epilepsy. Thus, the present study strongly suggests that PR and PL/(GCG)7 mutations independently cause lissencephaly